PHYSICAL REVIEW B **90**, 144101 (2014)

Atomic diffusion theory challenging the Cahn-Hilliard method

M. Nastar

CEA, DEN, Service de Recherches de Métallurgie Physique, F-91191 Gif-sur-Yvette, France

(Received 10 June 2014; revised manuscript received 22 September 2014; published 7 October 2014)

Our development of the self-consistent mean-field (SCMF) kinetic theory for nonuniform alloys leads to the statement that kinetic correlations induced by the vacancy diffusion mechanism have a dramatic effect on nanoscale diffusion phenomena, leading to nonlinear features of the interdiffusion coefficients. Lattice rate equations of alloys including nonuniform gradients of chemical potential are derived within the Bragg-Williams statistical approximation and the third shell kinetic approximation of the SCMF theory. General driving forces including deviations of the free energy from a local equilibrium thermodynamic formulation are introduced. These deviations are related to the variation of vacancy motion due to the spatial variation of the alloy composition. During the characteristic time of atomic diffusion, multiple exchanges of the vacancy with the same atoms may happen, inducing atomic kinetic correlations that depend as well on the spatial variation of the alloy composition. As long as the diffusion driving forces are uniform, the rate equations are shown to obey in this form the Onsager formalism of thermodynamics of irreversible processes (TIP) and the TIP-based Cahn-Hilliard diffusion equation. If now the chemical potential gradients are not uniform, the continuous limit of the present SCMF kinetic equations does not coincide with the Cahn-Hilliard (CH) equation. In particular, the composition gradient and higher derivative terms depending on kinetic parameters add to the CH thermodynamic-based composition gradient term. Indeed, a diffusion equation written as a mobility multiplied by a thermodynamic formulation of the driving forces is shown to be inadequate. In the reciprocal space, the thermodynamic driving force has to be multiplied by a nonlinear function of the wave vector accounting for the variation of kinetic correlations with composition inhomogeneities. Analytical expressions of the effective interdiffusion coefficient are given for two limit behaviors of the vacancy, the latter treated as either a conservative species (fixed concentration) or a nonconservative species (time-dependent equilibrium concentration). Relying on the same vacancy diffusion model, we perform kinetic Monte Carlo simulations starting from a sinusoidal composition modulation in binary model alloys, with no interaction or nearest-neighbor interactions leading to clustering or ordering tendencies, along the [100] crystallographic direction of a body centered cubic (bcc) lattice. The resulting temporal variation of the modulation amplitude is compared to the corresponding SCMF equations. Qualitative and satisfying quantitative agreements systematically strengthen our theoretical conclusions. The model alloys are shown to be representative enough of some real alloys, so that one may expect these new heterogeneous correlation effects to be non-negligible in these alloys.

DOI: 10.1103/PhysRevB.90.144101 PACS number(s): 66.30.Dn, 66.30.Ny, 05.10.Ln

I. INTRODUCTION

Up to now, there is no satisfying atomic theory of diffusion. The available ones are dedicated to the calculation of the phenomenological Onsager coefficients L_{ij}'s starting from an atomic scale description of the diffusion mechanism (see Ref. [1] for an extensive presentation of the various diffusion theories and recent developments of our self-consistent mean-field (SCMF) theory presented in Refs. [2–4]). The difficulty of evaluating the L_{ij}'s comes from the correlation effects. Indeed, diffusion in crystalline solids proceeds via the jumps of a few point defects on a lattice; as a consequence, the successive jumps of each given atom are kinetically correlated. Although the coefficients L_{ij}'s are equilibrium quantities, they are generally evaluated in systems out of equilibrium with driving forces assumed to be uniform. In alloys submitted to nonuniform driving forces, the relationship between the macroscopic diffusion properties and the atomic jump frequencies has not been established. In particular, the effect of driving force heterogeneities on the kinetic correlations has not received due attention. In systems where concentration heterogeneities have dimensions close to the interatomic distance, diffusion processes are expected to be strongly affected by the heterogeneous correlation effects. Therefore diffusion should be described at the atomic scale to get a good understanding of, for example, aging phenomena of nanoscale devices and bulk materials with nanoscale microstructures. Conventional diffusion experiments are conducted at spatial scales (decades of microns), which are too large to highlight the atomic scale features of diffusion. Instead, a few interdiffusion experiments performed on nanoscale composition-modulated foils have been performed. They are perfect for the characterization of atomic diffusion. A complex variation of the interdiffusion coefficient D with respect to the periodicity length of a sinusoidal composition-modulation has been observed—while at large wavelengths, a linear variation of D with squared wave vector k^2 is observed, at wavelengths smaller than a few lattice parameters an increasing slowing down of D with k^2 leads to a nonlinear function $D(k^2)$ (for a review see Ref. [5]).

Fick's second law, commonly used to study bulk diffusion, would predict a constant interdiffusion coefficient. Instead, phenomenological kinetic models including composition gradient-energy parameters such as the Cahn-Hilliard (CH) model lead to a linear variation of the effective interdiffusion coefficient with k^2 at small k [6,7]. Such models are based on a phenomenological expansion of the free energy of the solid solution written as a volume integral of a sum of local bulk and composition gradient energies [8]. They differ from a Fick's second law by the inclusion of this composition

gradient energy. The linear variation of the diffusion coefficient with k^2 is deduced from the k-space representation of the composition gradient energy, which in the diffusion coefficient appears as a gradient-energy parameter multiplied by k^2. The nonlinear behavior of the effective interdiffusion coefficient at short wavelength is not predicted by such phenomenological kinetic equations although they are used in nanoscale diffusion analysis, in phase field methods to simulate phase transformations starting from nanoscale composition fluctuations, and in spinodal decomposition theories to predict early stage kinetic laws [6,9,10].

This observation prompted the development of a microscopic version of the CH theory accounting for the atomic discrete aspect of the free energy, strongly inspired by the lattice rate kinetic equations introduced by Hillert [11]. Instead of using a coarse graining procedure, ensemble mean-field averages based on equilibrium statistical theories are used to calculate the discrete free energy [12–15]. The mean-field driving force leads to an effective interdiffusion coefficient nonlinear with k^2. Nonlinearity is due to the replacement of k^2 by discrete cosine operators of k associated with every interaction range and direction of diffusion [16]. Diffusion at the atomic scale is then predicted to be anisotropic even in a cubic lattice. Nonlinearities and anisotropy were even used to determine ordering parameters in solid solutions [17]. However, a few applications of this discrete kinetic theory to specific alloys were not fully convincing. The discrete driving force deduced from a thermodynamic database could not provide a clear explanation of the strong nonlinearity observed in the effective interdiffusion coefficients [18,19]. An alternative approach is to derive the whole atomic fluxes from ensemble averages not only the thermodynamic driving forces. The first derivation of the whole interdiffusion flux has been achieved by Martin [20]. The resulting microscopic expression has been shown to obey in this form the formalism of the CH method with a mobility depending on the local equilibrium composition and composition inhomogeneity. However, these atomic kinetic equations were derived for a microscopic direct exchange mechanism, which is a very rare mechanism in metallic alloys relative to the vacancy diffusion mechanism. For the vacancy diffusion mechanism, there have been some atomic derivations of the kinetic fluxes, though the kinetic correlations produced by the vacancy were neglected [21]. Eventually, all these microscopic mean-field theories like the Cahn-Hilliard approach yield an interdiffusion flux, which is written as a mobility multiplied by a thermodynamic formulation of the driving force. Within a phenomenological approach, the use of thermodynamics to derive nonequilibrium driving forces is justified by a local equilibrium hypothesis. This hypothesis leads to the statement that a thermodynamic expression of the free energy can describe very different states such as the equilibrium interface profile between two coexisting phases [8], the critical nucleus in a two-component metastable solid solution [22], multilayers and their stability against composition fluctuations [15,23,24], and also composition fluctuations of uniform systems and nonuniform systems during a phase decomposition [6,9].

However, in the case of uniform gradients of chemical potentials. The path probability method (PPM) and the SCMF theory showed that the phenomenological coefficients of the Onsager matrix for the vacancy diffusion mechanism [2–4,25–29] and the split interstitial diffusion mechanism [30–33] were correctly reproduced only if deviations of short-range order parameters from local equilibrium are taken into account. These deviations have been shown to be related to the kinetic correlations induced by the diffusion mechanism. They some time lead to spectacular kinetic phenomena such as percolation threshold phenomena [29] or solute drag by a vacancy flux [2–4]. In the specific case of vacancy diffusion mechanism, the kinetic correlations are produced by the higher probability of a given atom, after a first exchange with a vacancy, to exchange again with the same vacancy than exchange with a new vacancy, due to the small concentration of vacancy. Hence the jump sequence of an atom is not a random path and deviations from it correspond to the probability of a vacancy to make loop paths and a reverse jump with the atom. On the time scale of atomic diffusion, the effective probability of forming an exchanging atom-vacancy pair includes the probability of vacancy loop paths. Such probability related to the deviation of the exchanging pair probability from local equilibrium, depends on the kinetic parameters of the vacancy diffusion model and gradients of chemical potentials. The kinetic correlations of a composition-modulated foils resulting from the probability of a vacancy to leave, return and exchange again with the same atom, are expected to depend on the concentration field surrounding the atom and then on the wave vector k of the composition modulation as illustrated in Fig. 1. Note that PPM did not tackle this kinetic phenomenon because the few applications of PPM to phase transformations were restricted to order-disorder transitions, neglecting the effect of the spatial fluctuations of chemical potential gradients [34–38].

Our purpose is to start from an atomic scale description of the vacancy diffusion mechanism and extend the SCMF theory of diffusion to both nonsteady states and nonuniform gradients of chemical potential. A nonequilibrium distribution function represented by an exponential of time-dependent effective Hamiltonian is employed for the ensemble averaging, allowing a deviation of the state variables from local equilibrium values. The time-dependent effective Hamiltonian includes pair interactions beyond the first nearest-neighbor (1nn) atoms so that longer paths than the vacancy two-jump return paths are accounted for in the calculation of kinetic correlations. The ensemble averaging of the master equation yields nonlinear kinetic equation of the mean occupancies of a single site and pairs of sites. Application of a linear stability analysis should yield wavelength dependent effective interdiffusion coefficients which will be compared to direct atomic kinetic Monte Carlo simulations (AKMC). Body centered cubic (bcc) alloys with vacancy and nearest-neighbor interactions will be considered although the techniques can be generalized to any crystallographic structure and interactions among atoms separated by greater distances and other point defect diffusion mechanisms.

Section II introduces the SCMF kinetic theory, starting from a vacancy jump frequency model and yielding a set of nonlinear lattice rate equations. In Sec. III, the kinetic equations are explicitly written along the [100] crystallographic direction of a bcc lattice for various kinetic approximations.

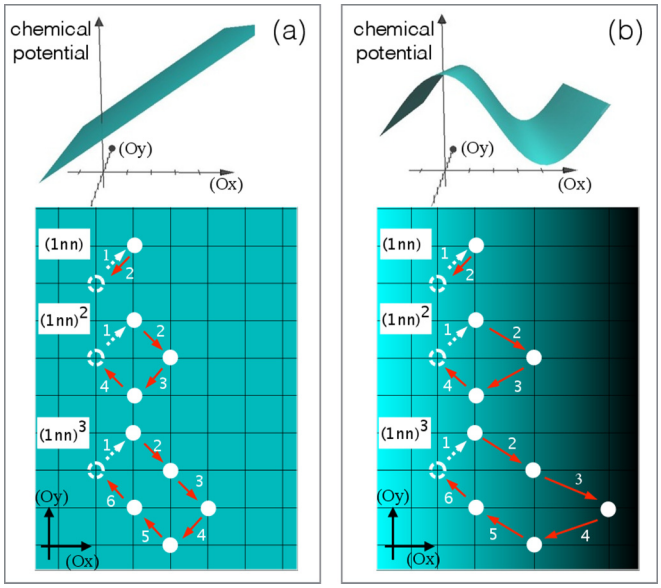

FIG. 1. (Color online) Spatial variation of the alloy chemical potential in a two-dimensional system (top), and short sequences of a two-dimensional walk of vacancy in (a) a uniform and (b) a nonuniform gradient of chemical potential. Typical loops of vacancy jump sequences are drawn, with a first jump starting from the dashed circle (white arrow) followed by a sequence of jumps (red arrows) exploring the neighboring sites of the dashed circle (white full circles) and a last jump leading to the dashed circle. For the calculation of the kinetic correlations, within a (1nn)-shell approximation, the loops exploring the 1nn sites of the dashed circle are included only, within a $(1nn)^2$ [respectively $(1nn)^3$] shell approximation, the 1nn of 1nn sites (respectively, 1nn of 1nn of 1nn) of the dashed circle are visited also. In (b), the length of vacancy jumps is artificially varied to illustrate the effect of chemical potential spatial variation on the vacancy jump frequencies and subsequently on the kinetic correlations. It is interesting to note that a (1nn)-shell kinetic approximation including vacancy two-jump paths only leads to kinetic correlations that do not depend on the spatial inhomogeneities of the chemical potential gradient.

The expression of the effective interdiffusion coefficient is derived from a stability analysis of the kinetic equations for two limit behaviors of the vacancy, the latter treated as a conservative species (fixed concentration) or nonconservative species (time dependent equilibrium concentration). In Sec. IV, atomic kinetic Monte Carlo (AKMC) simulations of kinetic decay of sinusoidal composition modulation along the ⟨100⟩ crystallographic direction of a bcc binary model alloy, with no interaction or nearest-neighbor positive and negative ordering energies, are performed. The resulting temporal variation of the modulation amplitude and measured effective diffusion coefficients are compared to the corresponding SCMF predictions. Then, general behaviors of the composition gradient and Laplacian terms of the interdiffusion coefficients are predicted by the SCMF theory. Eventually, a qualitative comparison of the kinetic properties between the chosen model alloys and a few real alloys is performed.

II. THE SELF-CONSISTENT MEAN-FIELD KINETIC THEORY

A. A vacancy jump frequency model

The large set of jump frequencies associated with species α in a concentrated alloy is assumed to follow a classical thermally activated form:

$$W_{ij}^{\alpha V} = \nu_\alpha \exp\left[-\beta\left(E_\alpha^{(s)} - \sum_{k,\zeta} \delta_{ik} V_{\alpha\zeta} \delta_k^\zeta\right)\right], \qquad (1)$$

where β is the inverse of the Boltzmann's constant multiplied by temperature T. ν_α is the attempt frequency depending on the jumping atom, and the term in the exponential is the migration enthalpy, that is, the difference between the total energy of the system in the initial configuration and when the jumping atom is at the saddle point. The migration energy is described by a breaking bond model limited to first nearest-neighbor (1nn) pair interactions. $E_\alpha^{(s)}$ is the contribution of the exchanging atom α to the saddle point energy. $E_\alpha^{(s)}$ is symmetric with respect to i and j so that the jump frequency model satisfies the detailed balance. The second term in the exponential corresponds to the sum of interaction energies $V_{\alpha\zeta}$ between the exchanging atom α and its neighbors ζ at the initial state. δ_{ik} is equal to 1 if lattice sites i and k are 1 nn. Occupation of a site i is specified by a set of occupation numbers (δ_i^α)—δ_i^α is equal to 1 if site i is occupied by α and 0 if else. This type of model was applied to real systems like the austenitic steels [39], the ferritic steels [40], and the aluminum alloys [41,42]. The present frequency model determines the transition probabilities from one alloy configuration to another one of a master equation, which is solved using AKMC simulations and the SCMF theory.

B. Atomic mean-field kinetic equations

In the present atomic diffusion theory, the independent variables used to describe nonuniform alloys include short-range order parameters in addition to the local concentration field and temperature, the volume and pressure being fixed in a rigid lattice model. In the present study, short-range order parameters are limited to the mean occupancy of pairs of neighboring sites (pair probability) and the local concentration field is described at the atomic scale by the mean occupancy of single sites. The introduction of a nonequilibrium distribution function yields mean-field kinetic equations for the mean occupancy of sites as well as for the deviation of pair probabilities from a local equilibrium relationship. The nonequilibrium distribution function is written after the equilibrium distribution function P_0 multiplied by a nonequilibrium distribution function P_1 written as an exponential of a time-dependent effective Hamiltonian $h(t)$ converging to zero at equilibrium:

$$h(t) = \frac{1}{2} \sum_{\alpha\zeta, i\neq j} v_{ij}^{\alpha\zeta}(t) \delta_i^\alpha \delta_j^\zeta. \qquad (2)$$

The effective pair interactions $v_{ij}^{\alpha\zeta}$ between an atom α on site i and an atom ζ on site j are unknown and must be obtained solving the master equation. Previous developments

of the SCMF theory focused on the steady state solutions of the master equation. It was to calculate the phenomenological coefficients associated with the vacancy mechanism [2–4,27–29] and the interstitial mechanism [30–33]. Two hierarchies of approximations may be explored. The first one is determined by the number of effective interactions used to define the nonequilibrium distribution function. It determines the number of kinetic equations to be solved. The second level of approximation concerns the statistical approximation used to calculate the equilibrium ensemble averages of the jump probabilities. In the present work, three kinetic approximations are investigated, the first-shell one with an effective Hamiltonian $\widehat{h}$ restricted to 1nn effective pair interactions, the second shell one with $\widehat{h}$ restricted to 1nn and 1nn of 1nn pair interactions [$(1nn)^2$ approximation], and the third shell one with $\widehat{h}$ restricted to 1nn, 1nn of 1nn and 1nn of 1nn of 1nn pair interactions [$(1nn)^3$ approximation]. For the thermodynamic approximation used to calculate the jump probabilities, a statistical Bragg-Williams (BW) point approximation is employed. Same approximations have already been used to find the steady-state solution of a system submitted to a uniform chemical potential gradient in Ref. [27]. This work is an extension of Ref. [27] to transitory kinetics of systems described by nonuniform gradients of chemical potentials. In that case, the relationship between the effective interactions and the pair probabilities has to be made explicit. Starting from the definition of a pair probability occupation of sites i and j by species α and ζ:

$$\left\langle \delta_i^\alpha \delta_j^\zeta \right\rangle = \sum_{\mathbf{n}} \delta_i^\alpha \delta_j^\zeta \widehat{P}_0(\mathbf{n}) \widehat{P}_1(\mathbf{n},t) = \left\langle \delta_i^\alpha \delta_j^\zeta P_1(\mathbf{n},t) \right\rangle^{(0)}, \quad (3)$$

where the exponent $^{(0)}$ indicates that the ensemble average corresponds to an equilibrium average, which here will be calculated by means of a mean-field BW approximation. We deduce an expression of the pair correlator at first order in the pair effective interactions:

$$\begin{aligned} k_{ij}^{\alpha\zeta} &= \left\langle \delta_i^\alpha \delta_j^\zeta \right\rangle - c_i^\alpha c_j^\zeta \\ &= c_i^\alpha c_j^\zeta \beta \left(h_{ij}^\alpha + h_{ji}^\zeta - h_{ij}^{\alpha\zeta} - \sum_{\alpha\zeta} h_{ij}^{\alpha\zeta} c_i^\alpha c_j^\zeta \right), \end{aligned} \quad (4)$$

where $c_i^\alpha = \langle \delta_i^\alpha \rangle$ is the mean occupation of site i by species α, the formal derivative $h_{ij}^{\alpha\zeta}$ is equal to $v_{ij}^{\alpha\zeta}$ and h_{ij}^α reads

$$h_{ij}^\alpha = \sum_\zeta v_{ij}^{\alpha\zeta} c_j^\zeta. \quad (5)$$

Note that Eq. (4) satisfies the normalization condition of the pair probabilities: the sum over ζ of the pair correlator is zero hence the sum over ζ of probabilities $\langle \delta_i^\alpha \delta_j^\zeta \rangle$ is equal to the on-site mean concentration c_i^α. Equation (4) can be used to express the effective interactions in terms of the pair correlators. The unknown variables associated with a pair of sites (i,j) occupied by species α and ζ are then represented by $A_{ij}^{\alpha\zeta}$ and $S_{ij}^{\alpha\zeta}$, where $A_{ij}^{\alpha\zeta} = k_{ij}^{\alpha\zeta} - k_{ij}^{\zeta\alpha}$ is the antisymmetric pair correlator and $S_{ij}^{\alpha\zeta} = k_{ij}^{\alpha\zeta} + k_{ij}^{\zeta\alpha}$ is the symmetric pair correlator.

In a binary alloy AB with vacancy V, a pair of sites can be occupied by (A,A), (A,V), (B,V), (A,B), (BB), or (VV). However, the normalization of the distribution function applied to the pair probabilities implies relationships between the pair correlators and pairs VV are neglected due to the small vacancy concentration, reducing the set of independent pair correlators of a given pair of sites (i,j) to the threefold ensemble $(A_{ij}^{AB}, S_{ij}^{AB}, S_{ij}^{AV})$.

Rate equation of the mean occupation of site i by species α is written at first order in $\delta\mu$ and the effective Hamiltonian $\widehat{h}$:

$$\begin{aligned} \frac{d\langle \delta_i^\alpha \rangle}{dt} = \beta \sum_s \delta_{is} \big\langle & \widehat{W}_{si}^{\alpha V} \delta_s^\alpha \delta_i^V \left(\delta\mu_s^\alpha + \delta\mu_i^V - \widehat{h}_s^\alpha - \widehat{h}_i^V \right) \\ & - \widehat{W}_{si}^{V\alpha} \delta_s^V \delta_i^\alpha \left(\delta\mu_s^V + \delta\mu_i^\alpha - \widehat{h}_s^V - \widehat{h}_i^\alpha \right) \big\rangle^{(0)}, \end{aligned} \quad (6)$$

where $\widehat{h}_i^\alpha$ is the formal partial derivative of $\widehat{h}$ with respect to δ_i^α. δ_{ij} is equal to zero unless site i and j are 1nn sites. Due to the following relation: $\delta_i^\alpha \delta_i^\zeta = \delta_{\alpha\zeta}^{Kr} \delta_i^\alpha$, where $\delta_{\alpha\zeta}^{Kr}$ is equal to 1 if $\alpha = \zeta$ and 0 if else (Kronecker symbol), as it is explained in Refs. [27,29], a Bragg-Williams approximation of Eq. (6) yields

$$\begin{aligned} \frac{d\langle \delta_i^\alpha \rangle}{dt} = L_{\alpha\alpha}^{(0)} \beta \sum_s \delta_{is} \big[& \left(\mu_s^{\alpha V} - \mu_i^{\alpha V} \right) \\ & - \left(h_{is}^\alpha + h_{si}^V - h_{is}^{\alpha V} - h_{si}^\alpha - h_{is}^V + h_{is}^{V\alpha} \right) \big], \end{aligned} \quad (7)$$

where the nonequilibrium chemical potential is defined by the relation: $\mu_s^{\alpha V} = \delta\mu_s^\alpha - \delta\mu_s^V + h_s^\alpha - h_s^V$. The particular feature to be noted in our previous diffusion papers and the present one, is that it is not necessary to assume, but rather the theory derives, that the gradients of local chemical potentials are the driving forces for the fluxes. Furthermore, these local non-equilibrium chemical potentials are shown to be related to the local concentrations through a thermodynamic relationship [28]. Formal derivatives of the effective hamiltonian appearing in the second line of Eq. (7) can be interpreted as additional driving forces to the classical chemical potential ones.

$L_{\alpha\alpha}^{(0)}$ corresponds to an ensemble average of the jump frequency calculated in the homogeneous equilibrium state for which chemical potential gradients are zero and nominal concentration of species i is c_i:

$$L_{ii}^{(0)} = c_i c_V \nu_i \exp\left\{ -\beta \left[E_i^{(s)} - Z \sum_\zeta (V_{i\zeta} + V_{i\zeta}) c_\zeta \right] \right\}, \quad (8)$$

where Z is the number of 1 nn (equal to eight in a bcc alloy).

By means of Eq. (4), Eq. (7) is written in terms of pair correlators as

$$\frac{d\langle \delta_i^\alpha \rangle}{dt} = L_{\alpha\alpha}^{(0)} \beta \sum_s \delta_{is} \left(\mu_s^{\alpha V} - \mu_i^{\alpha V} - \frac{A_{is}^{\alpha V}}{c_\alpha c_V} \right). \quad (9)$$

This rate equation is found to depend on the 1nn antisymmetric pair correlators only. Note that the detailed balance has been used to factorize $L_{\alpha\alpha}^{(0)}$.

Since the procedure is similar to that for solving the kinetics of a single site mean occupation, $\langle \delta_i^A \rangle$, we skip some of the steps and obtain for the antisymmetric pair correlator,

$$\begin{aligned} \frac{dA_{ij}^{AV}}{dt} = & 2\delta_{ij} \left(c_B L_{AA}^{(0)} \nabla\beta\mu_i^{AV} - c_A L_{BB}^{(0)} \nabla\beta\mu_i^{BV} \right) \\ & - \left[2q_2\delta_{ij} + (Z - \delta_{ij}) q_0 \right] A_{ij}^{AV} \end{aligned}$$

$$-\frac{q_0}{2}\sum_k\left(\delta^i_{jk}A^{AV}_{jk}-\delta^j_{ik}A^{AV}_{ik}\right)$$
$$-\frac{q_0}{2}\sum_k(\delta^i_{jk}S_{jk}-\delta^j_{ik}S_{ik}), \quad (10)$$

where δ^i_{jk} is equal to zero unless sites j and k are 1nn sites and k is different from i. ∇ corresponds to the discrete gradient operator. q parameters are given by

$$\begin{aligned} q_0 &= \left(L^{(0)}_{AA}+L^{(0)}_{BB}\right)/c_V \\ q_1 &= \left(c_BL^{(0)}_{AA}-c_AL^{(0)}_{BB}\right)(c_Ac_Bc_V) \\ q_2 &= \left(c^2_BL^{(0)}_{AA}+c^2_AL^{(0)}_{BB}\right)/(c_Ac_Bc_V). \end{aligned} \quad (11)$$

S_{ik} is a symmetric combination of pair correlators defined by

$$S_{ik}=S^{AV}_{ik}+\frac{q_1}{q_0}c_vS^{AB}_{ik}. \quad (12)$$

In the case of a uniform gradient of chemical potential, due to the translation symmetry of the effective interactions, the pair correlators of sites i and j depend on the difference $(j-i)$ only and last sum of Eq. (10) involving the symmetric pairs S_{jk} and S_{ik} is null. Then the kinetics of the concentration field is coupled to the antisymmetric pair correlators A^{AV}_{ij} only and solution is derived from the time integration of the reduced system of equations combining Eqs. (9) and (10). Note that the coefficients in front of the antisymmetric correlator A^{AB}_{ij} are not proportional to c_v, which leads to a characteristic time of the antisymmetric pair c_v times smaller than the characteristic time of the atomic concentration fields. The relaxation kinetics of the vacancy pair correlators are thus assumed to be instantaneous with respect to the concentration field kinetics. The latter approximation is equivalent to applying an adiabaticity approximation to the rate equation of the vacancy pair correlators and put Eq. (10) equal to 0. It is interesting to note that the resulting antisymmetric pair correlators, i.e., the deviation of short-range order from local equilibrium, are uniform and proportional to the chemical potential gradients. Then the replacement of $A^{\alpha V}_{is}$ in Eq. (9) by its expression in terms of chemical potential gradients leads to a discrete version of the TIP rate equations.

In the case of nonuniform gradients of chemical potential, kinetics of the antisymmetric and symmetric pair correlators are coupled. First, we consider the time derivative of S^{AV}_{ij}:

$$\frac{dS^{AV}_{ij}}{dt}=-(Z-\delta_{ij})S_{ij}+\frac{q_0}{2}\sum_k\left(\delta^i_{jk}S_{jk}+\delta^j_{ik}S_{ik}\right)$$
$$-\frac{q_0}{2}\sum_k\left(\delta^i_{jk}A^{AV}_{jk}+\delta^j_{ik}A^{AV}_{ik}\right). \quad (13)$$

As for the antisymmetric pair correlator, the coefficient in front of S^{AV}_{ij} is not proportional to c_v and an adiabatic approximation is applied to Eq. (13) as well. Contrary to the case of uniform chemical potentials, both the chemical potential gradients and the set of unknown variables, $(c^A_i,c^B_i,A^{AB}_{ij},S_{ij})_{ij}$ depend on their spatial coordinates i and j, and they are fully determined by the system of equations combining Eqs. (7), (10), and (13). Note that the rate equation of the third independent pair correlator S^{AB}_{ij} is required to describe the kinetics of the atom-atom pair correlators:

$$\frac{dS^{AB}_{ij}}{dt}=-(Z-\delta_{ij})S'_{ij}+\frac{q'_0}{2}\sum_k\left(\delta^i_{jk}S'_{jk}+\delta^j_{ik}S'_{ik}\right)$$
$$-\frac{q'_0}{2}\sum_k\left(\delta^i_{jk}A^{AV}_{jk}+\delta^j_{ik}A^{AV}_{ik}\right), \quad (14)$$

where

$$S'_{ik}=S^{AV}_{ik}+\frac{q'_1}{q'_0}c_vS^{AB}_{ik} \quad (15)$$

and

$$\begin{aligned} q'_0 &= \left(L^{(0)}_{AA}-L^{(0)}_{BB}\right)/c_V \\ q'_1 &= \left(c_BL^{(0)}_{AA}+c_AL^{(0)}_{BB}\right)(c_Ac_Bc_V). \end{aligned} \quad (16)$$

S^{AB}_{ij} represents the fluctuations of the symmetric part of the atomic pair correlator k^{AB}_{ij}, hence contributing to the concentration fluctuations around a homogeneous solid solution of nominal concentrations c_A and c_B:

$$\left\langle\left(\delta^A_i-c_A\right)\left(\delta^B_j-c_B\right)\right\rangle=\left(c^A_i-c_A\right)\left(c^B_i-c_B\right)$$
$$+0.5\left(S^{AB}_{ij}+A^{AB}_{ij}\right), \quad (17)$$

where A^{AB}_{ij} can be neglected because a resolution of Eqs. (10), (13), and (14) would easily show that A^{AB}_{ij} is c_V times smaller than S^{AB}_{ij}. The contribution of S^{AB}_{ij} is essential when $(c^A_i-c_A)(c^B_i-c_B)$ is small as for instance in the beginning of a sinusoidal decomposition. If one studies the decay of a sinusoidal concentration profile with a sufficiently large amplitude, S^{AB}_{ij} can be neglected.

To conclude, the evolution of the concentration profile is essentially determined by the kinetics of the mean concentration field, which is the solution of Eq. (7). The latter depends on the time-dependent antisymmetric pair correlator A^{AV}_{is} between 1nn sites i and s. In the case of uniform chemical potential gradients, the kinetics of A^{AV}_{is} depends on the antisymmetric pair correlators (A^{AV}_{ij}), which are the solution of Eq. (10). The resulting antisymmetric pair correlators are uniform. Instead, in the case of nonuniform chemical potential gradients, in addition to (A^{AV}_{ij}), the 1nn antisymmetric pair correlator A^{AV}_{is} depends on the symmetric combinations of pair correlators (S_{ik}) defined by Eq. (12); the pair variables (A^{AV}_{ij}) and (S_{ik}) being solutions of Eqs. (10) and (13).

III. DIFFUSION EQUATIONS

Diffusion equations are written for a bcc lattice. First, a nomenclature of pair correlators is introduced to treat the specific case of a 1D-sinusoidal concentration field along a given direction. Then a stability analysis with a sinusoidal concentration fluctuation directed along the [100] direction of the bcc crystal is presented, first within the first-shell (1nn) kinetic approximation, then within the second $(1nn)^2$ and third $(1nn)^3$-shell approximations. In the next section, the rate equations and the resulting interdiffusion coefficient are derived in the case of nonconservative vacancy. Eventually, a Taylor expansion of the diffusion coefficient with respect to the wave vector leads to an interpretation of the kinetic correlations as correction terms of the Cahn-Hilliard driving force.

A. Nomenclature of the pair variables

The independent classes of pair variables to be considered depend on the applied chemical potential and the kinetic approximation used to solve the rate equations. In the specific case of a 1D-sinusoidal concentration field along a given direction (Ox), it is convenient to project the kinetic equations along (Ox) and use the 1D symmetry to reduce the number of relevant variables. First, the chemical potential gradient is aligned along (Ox). Considering a unit vector $\vec{u}$ along (Ox), two pairs of sites ij and $i'j'$ that have the same length and the same projection on vector $\vec{u}$ belong to the same class. However, in contrast to the case of a uniform chemical potential gradient, the pair correlators associated with ij and ji are not antisymmetric and the classes of bonds normal to $\vec{u}$ do not cancel out. Moreover, there is no translational symmetry and the pair $i'j'$ is defined by its belonging to the class ij and its coordinate $x_{i'}$ on axis (Ox): $x'_i = (\vec{Oi'}.\vec{u})/d$, where O is a reference point and d is the interplane distance along (Ox). In the following, we use $\vec{e}_{is}$ to designate the unit vector linking sites i and s and for any class we choose a representative $\bar{i}\,j$ whose projection on (Ox) is positive. The pair ik will be noted $(x_i,\bar{m}\,j)$ if the pair ik belongs to the class of mj and $\vec{e}_{ik}.\vec{u} \geqslant 0$, and $(x_k,\bar{m}\,j)$ if the pair ik belongs to the class of mj and $\vec{e}_{ik}.\vec{u} \leqslant 0$.

In practice, a finite number of pairs are considered. In the first (1nn)-shell approximation, a single class associated with 1nn pairs noted 1 is considered. An nn pair occupied by species (α,ζ) is then represented by two independent pair correlators: the antisymmetry correlator $A^{\alpha\zeta}_{i,1} = k^{\alpha\zeta}_{i,1} - k^{\zeta\alpha}_{i,1}$ and the symmetric correlator $S^{\alpha\zeta}_{i,1} = k^{\alpha\zeta}_{i,1} + k^{\zeta\alpha}_{i,1}$. Similarly, the symmetric combination of 1nn pair correlators defined in Eq. (12) is represented by $S_{i,1}$. In the $(1nn)^2$-shell approximation, pairs between a given site and 1nn sites of its 1nn sites are kept. In the specific case of a vector $\vec{u}$ aligned along the [100] direction of the bcc crystal, representative members of the pairs are respectively the first, second, third, fifth nn bonds, which are noted, 1, 2, 3, and 5. Note that besides these pairs, pairs lying in planes perpendicular to $\vec{u}$ have to be considered. Representative members of bonds normal to $\vec{u}$ between respectively the second and the third nn sites are noted $P_{i,2}$ and $P_{i,3}$, where i is the x coordinate. A schematic representation of the bonds and pair correlators to be considered in the (1nn), $(1nn)^2$, and $(1nn)^3$-shell approximations is shown in Fig. 2.

B. Stability analysis

In a binary alloy AB submitted to a local gradient of chemical potential, the rate equation of the concentration field [Eq. (9)] is written for c^A_i and c^B_i along the direction of the chemical potential gradient (Ox)

$$\begin{aligned}\frac{dc^A_i}{dt} &= z_d L^{(0)}_{AA}\nabla^2\beta\mu^{AV}_i - z_d L^{(0)}_{AA}\nabla\frac{A^{AV}_{i,1}}{c_A c_V}\\ \frac{dc^B_i}{dt} &= z_d L^{(0)}_{BB}\nabla^2\beta\mu^{BV}_i + z_d L^{(0)}_{BB}\nabla\frac{A^{AV}_{i,1}}{c_B c_V},\end{aligned} \tag{18}$$

where z_d is the number of 1nn sites with same x coordinate. ∇^2 corresponds to the discrete Laplacian operator. $A^{\alpha V}_{i,1}$ is then calculated by means of Eqs. (10) and (13) involving the symmetric pair correlators and longer range antisymmetric pair correlators.

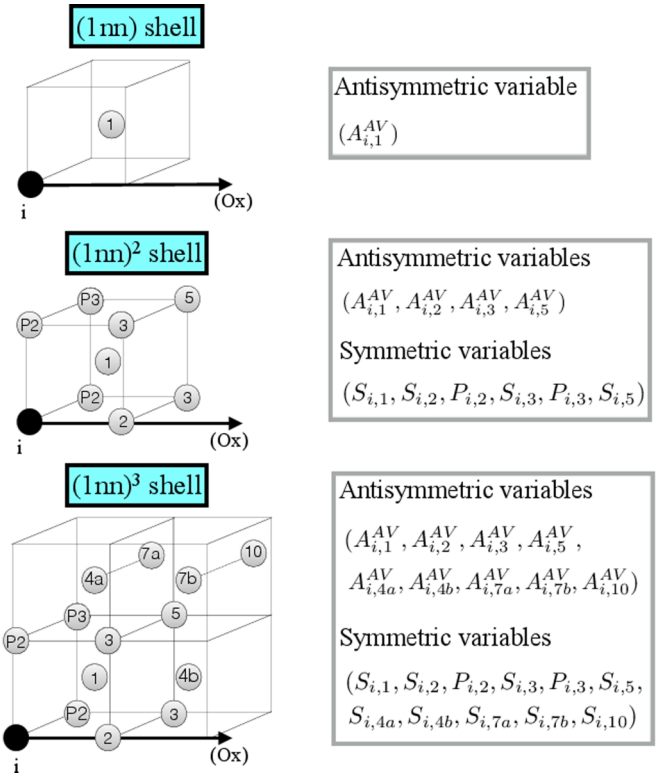

FIG. 2. (Color online) Representation of the bonds formed by the atom (black disk with x coordinate i) and one of its neighbors to be considered in the (1nn), $(1nn)^2$, and $(1nn)^3$-shell approximations. Letter P is added to the nomenclature of bonds 2 and 3 lying in the plane perpendicular to the axis (Ox) (direction of the chemical potential gradient). Letters a and b are added to the nomenclature of bonds 4 and 7 when their x coordinates are different. The unknown pair correlators to be calculated are listed on the right column. Note that there is no antisymmetric contributions to the perpendicular bonds $P2$ and $P3$; and within the (1nn)-shell contribution, the symmetric 1nn pair correlator $S_{i,1}$ is not listed because it is not involved in the rate equations to be solved [Eqs. (18) and (19)].

The stability analysis of the rate equations is presented in detail for the first-shell (1nn) kinetic approximation. Within a (1nn)-shell approximation, 1nn pairs are considered only. The time derivative of the 1nn antisymmetric pair correlator is derived from Eq. (10) as follows:

$$\begin{aligned}\frac{dA^{AV}_{i,1}}{dt} &= 2\left(c_B L^{(0)}_{AA}\nabla\beta\mu^{AV}_i - c_A L^{(0)}_{BB}\nabla\beta\mu^{BV}_i\right)\\ &\quad - [2q_2 + (Z-1-Q_\Lambda)q_0]A^{AV}_{i,1}.\end{aligned} \tag{19}$$

Application of the adiabatic approximation on Eq. (19) yields an expression of the nonequilibrium antisymmetric pair correlator $A^{AV}_{i,1}$ in terms of the chemical potential gradients. $A^{AV}_{i,1}$ is then governed by the difference between two distinct driving forces, respectively proportional to $\nabla\beta\mu^{AV}_i$ and $\nabla\beta\mu^{BV}_i$, traducing the fact that a vacancy jump sequence is driven by a competition between A-V and B-V exchanges (the so-called correlation effects). The larger the competition, the larger the deviation of antisymmetric pair probabilities

from the local equilibrium value and the larger the kinetic correlations. The time variation of the concentration fields is then fully determined by the closed set of rate equations formed by Eqs. (18) and (19). When the expression of $A_{i,1}^{AV}$ is introduced into Eq. (18), the rate equations obey in this form the formalism of thermodynamics of irreversible processes (TIP) of Onsager (see, for example, Ref. [1]). By identification with the macroscopic TIP equations, the driving forces are identified as partial derivatives of the discrete free energy function and the phenomenological coefficients are equal to

$$\begin{aligned} L_{AB} &= \frac{2L_{AA}^{(0)}L_{BB}^{(0)}}{c_v[q_0(Z-1-Q_\Lambda)+2q_2]} \\ L_{AA} &= L_{AA}^{(0)}\left(1-c_B\frac{L_{AB}}{c_A L_{BB}^{(0)}}\right) \\ L_{BB} &= L_{BB}^{(0)}\left(1-c_A\frac{L_{AB}}{c_B L_{AA}^{(0)}}\right), \end{aligned} \tag{20}$$

where constant Q_Λ is equal to zero within the present (1nn)-shell approximation. As observed in Eq. (18), the off-diagonal phenomenological coefficient L_{AB} is directly related to the 1nn antisymmetric pair correlator and would be equal to zero if deviations of the 1nn pair probabilities from local equilibrium were not considered. Within a (1nn)-shell approximation, kinetic correlations result from the probability of the vacancy to perform a reverse jump just after a given AV exchange. Such two-jump loops lead to coefficients L_{ij}, which do not depend on the shape of the concentration field. Instead, N-jump loops with $N > 2$ make the vacancy explore the concentration field and are expected to produce kinetic correlations depending on the wave vector of the concentration modulation. The schematic of Fig. 1 gives a visual idea of the respective contributions of a two-jump loop and multiple-jump loops to the kinetic correlations.

Following the CH approach, Eqs. (18) and (19) are linearized at first order in concentration fluctuations and Fourier transformed to get a system of linear equations. The Fourier transform of the composition fluctuation $[c_\alpha(x,t)-c_\alpha]$ around the average composition c_α at wave vector k is noted $\delta c_\alpha(k)$. The linearization of the chemical potentials at first order in concentration fluctuations reads

$$\begin{aligned} \delta\mu_{AV}(k) &= TF\left\{\mu_i^{AV}-\mu_{AV}\right\} \\ &= T_{AA}(k)\delta c_A(k)+T_{AB}(k)\delta c_B(k), \end{aligned} \tag{21}$$

where μ_{AV} is the chemical potential difference $(\mu_A-\mu_V)$ in the homogeneous equilibrium state. The resulting kinetic equations in the reciprocal space become then a linear system of equations:

$$\begin{aligned} \frac{d\delta c_A(k)}{dt} &= -\Lambda(k)L_{AA}(T_{AA}\delta c_A+T_{AB}\delta c_B) \\ &\quad -\Lambda(k)L_{AB}(T_{BA}\delta c_A+T_{BB}\delta c_B) \\ \frac{d\delta c_B(k)}{dt} &= -\Lambda(k)L_{BB}(T_{BA}\delta c_A+T_{BB}\delta c_B) \\ &\quad -\Lambda(k)L_{BA}(T_{AA}\delta c_A+T_{AB}\delta c_B). \end{aligned} \tag{22}$$

A linear stability analysis of these microscopic TIP equations provides the atomic on-site concentrations depending on two exponentials. The first exponential is related to the vacancy relaxation kinetics with a frequency $R_V=-\Lambda(k)(L_{AA}+L_{BB}+2L_{AB})/c_V$. The second exponential frequency R is found to be the product of a mobility M multiplied by a discrete CH driving force $\Phi_{\rm CH}^\Lambda$:

$$R=-M\Lambda\Phi_{\rm CH}^\Lambda, \tag{23}$$

where

$$\Phi_{\rm CH}^\Lambda=c_V(T_{AA}T_{BB}-T_{AB}T_{BA}). \tag{24}$$

When interactions are limited to 1nn interactions, the driving force can be written as $\Phi_{\rm CH}^\Lambda=f''+\kappa_E\Lambda(k)$, where f'' is the second derivative of the binary alloy free energy with respect to concentration and κ_E is the gradient energy coefficient [8]. Mean-field approximations of these parameters are presented in Appendix A. The squared wave number $(ak)^2$ (where a is the lattice parameter) of the continuous CH equation is replaced by the wave-vector discrete operator

$$\Lambda(k)=-z_d(2\cos kd-2), \tag{25}$$

where d is the interplanar spacing [$d=a/2$ in the [100] direction of the bcc crystal]. $\Lambda(k)$ tends to $(ak)^2$ at small (ak) and $\Lambda(k)=16$ when $ak=2\Pi$ and wavelength $\lambda=a$. Inside the spinodal region, f'' is negative and the frequency R is positive for all wave vectors smaller than a critical wave vector k_c. k_c is the wave vector at which $\Lambda(k_c)=\Lambda_c$, Λ_c being deduced from the equality $f''+\kappa_E\Lambda_c=0$. Concentration fluctuations with a wave vector below k_c will be amplified exponentially with aging time. However, except for the example plotted in Fig. 14, the application of the present theory is restricted to homogeneous equilibrium solid solutions with positive f''. Thus R is negative whatever the wave vector and a sinusoidal concentration profile decays with aging time.

Mobility M is found to be equal to

$$M=\frac{L_{AA}L_{BB}-L_{AB}^2}{L_{AA}+L_{BB}+2L_{AB}}, \tag{26}$$

where, the coefficients L_{ij} correspond to the first-shell kinetic approximation of the phenomenological Onsager coefficients as given by Eq. (20). The mobility M is not the interdiffusion-related mobility that is currently used in the phase field method. The present effective interdiffusion coefficient is equal to

$$D=-\frac{R}{\Lambda}=M\Phi_{\rm CH}^\Lambda. \tag{27}$$

Note that in Eq. (27), the pulsation R is chosen to be divided by the dimensionless wave-vector operator Λ instead of the squared wave vector k^2, leading to units of D equal to (s^{-1}) instead of the classical units ($m^2.s^{-1}$).

The kinetics of the atomic concentration fields is mainly controlled by the atomic pulsation R because the latter is c_V times smaller than the vacancy relaxation rate R_V. Therefore, when a vacancy is treated as a conservative species, the reaction is controlled by a single diffusion coefficient defined in Eq. (27). Differences between conservative and nonconservative vacancy diffusion will be described in Sec. III D.

C. Beyond the first-shell kinetic approximation

A first-shell (1nn) kinetic approximation implies the calculation of a single effective pair interaction, the 1nn

antisymmetric pair correlator $A_{i,1}$, from Eq. (10). Beyond this approximation, both symmetric and antisymmetric contributions of pair correlators are involved as they both appear in Eq. (10). In addition to Eq. (10) associated with the antisymmetric pair derivative, Eq. (13) associated with the symmetric pair derivative is then needed to get a closed system of equations SE. As explained in Appendix B, expressions of the unknown symmetric and antisymmetric pair correlators are a solution of SE. Every pair correlator is a linear combination of gradients of chemical potential and participates to the deviation of pair probabilities from their local equilibrium values. The resulting kinetic equations for the concentration fields are similar to Eq. (22) except that the parameter Q_Λ entering Eq. (20) is different from zero and is a function of the wave vector Λ. The coefficients L_{ij} defined in Eq. (20) are then replaced by the wave vector dependent coefficients L_{ij}^Λ. Within a $(1nn)^2$-shell kinetic approximation, the calculation of Q_Λ detailed in Appendix B leads to

$$Q_\Lambda = 7 - \frac{1269}{10\Lambda + 216}. \tag{28}$$

The same parameter calculated within the third shell [also called $(1nn)^3$-shell] kinetic approximation reads

$$Q_\Lambda = 7 - \frac{11\,190\,404\,097}{333\,389\,461\Lambda + 2\,008\,131\,183}. \tag{29}$$

As k tends to zero, Λ tends to zero and the kinetic coefficients L_{ij}^Λ tend to the phenomenological kinetic coefficients L_{ij} of the Onsager matrix. At finite Λ, L_{ij}^Λ is a function of the wave vector of the driving force and should not be interpreted as a phenomenological transport coefficient. The contribution of Λ to the kinetic correlations and L_{ij}^Λ arises from long-range vacancy loops (cf. Fig. 1). In a (1nn)-shell approximation, the 1nn pair correlator describes the two-jump vacancy loops corresponding to a series of first and reverse jumps between the initial sites of the exchanging pair. These two-jump loops make the vacancy explore local gradients of chemical potential. In a $(1nn)^2$-shell approximation, the vacancy loops corresponding to a series of jumps starting from the first site, reaching 1nn of 1nn of the initial site and ending on the first site, make the vacancy explore the local curvature of chemical potentials. The exploration of Λ-dependent curvature and higher-order derivatives of chemical potentials yields the Λ-dependent L_{ij}^Λ (as illustrated in Fig. 1). However, this contribution due to an interplay between kinetic correlations and the spatial variation of driving forces could also be interpreted as a deviation of driving forces from a thermodynamic formulation. The effective local chemical potential gradient of unstable solid solutions would depend not only on the local concentration but also on new independent state variables, the atomic pair correlations. Whatever the interpretation we have of these wave-vector dependent kinetic correlations, the resulting atomic mean-field equations do not obey the formalism of TIP: fluxes are no more written as linear combinations of Lij-chemical potential gradient products. Each product is now multiplied by a wave-vector dependent correlation coefficient (L_{ij}^Λ/L_{ij}). Note that the resulting fluxes are still vanishing at equilibrium, i.e., when the thermodynamic driving forces are null. Moreover, in the case of uniform chemical potential gradients, the TIP formalism is recovered. Indeed, the wave-vector contribution to the kinetic correlations arises with the heterogeneities of the chemical potential gradients. Therefore when the chemical potential gradients are uniform, the L_{ij}^Λ coefficients are equal to $L_{ij}^\Lambda(\Lambda = 0) = L_{ij}$.

As for the (1nn)-shell approximation, the atomic relaxation rate R is deduced from Eq. (23) in which the phenomenological Onsager coefficients L_{ij} are replaced by wave-vector dependent coefficients L_{ij}^Λ. For the sake of clarity, the wave-vector dependent contribution to the effective mobility is introduced as a heterogeneous correlation coefficient:

$$f_\Lambda = \frac{M(\Lambda)}{M}, \tag{30}$$

where $M(\Lambda)$ (respectively, M) is derived from Eq. (26) at finite Λ (respectively, at $\Lambda = 0$). Note that the coefficients L_{ij} used to calculate the mobility M correspond either to the $(1nn)^2$- or to the $(1nn)^3$-shell approximation of the macroscopic Onsager coefficients. The variation of the effective interdiffusion coefficient D and the corresponding pulsation R against Λ are then determined by the thermodynamic driving force Φ_{CH}^Λ, as well as the heterogeneous correlation coefficient f_Λ,

$$\begin{aligned} D &= M f_\Lambda \Phi_{CH}^\Lambda \\ R &= -\Lambda M f_\Lambda \Phi_{CH}^\Lambda. \end{aligned} \tag{31}$$

Whatever the kinetic approximation and the wave vector, Q_Λ is positive and f_Λ is below one. Therefore, in a stable solid solution with positive Φ_{CH}^Λ, the heterogeneous correlation coefficient systematically lowers D and increases R. Note that in the case of uniform chemical potential gradients, the heterogeneous correlation coefficient is equal to $f_\Lambda(k = 0) = 1$ and a CH-like formulation of D is regained.

D. Vacancy as a conservative or nonconservative species

Up to now, the vacancy was considered a conservative species, meaning that the nominal vacancy concentration of the system is fixed and does not vary with time. In the classical models for diffusive phase transformations, it is usually assumed that the vacancy is a nonconservative species that is at local equilibrium, meaning that its local concentration is instantaneously modified to reach the equilibrium vacancy concentration of a homogeneous alloy with a nominal composition equal to the local atomic composition. Conservative and nonconservative vacancy limit cases as well as intermediate cases are encountered in real systems. Below, the difference between both limit cases is investigated.

When the vacancy is treated as a conservative species, the number of sites is conserved and the vacancy concentration fluctuation is related to the atomic ones: $\delta c_V = -\delta c_A - \delta c_B$. Applying the same relationships for the time derivatives, the vacancy rate equation is deduced from Eq. (22). Application of the adiabatic approximation to the vacancy rate equation relates the vacancy concentration fluctuation to the atomic concentration fluctuation of species A:

$$\begin{aligned} \frac{\delta c_V}{c_V} = &\frac{(L_{AA}^\Lambda + L_{AB}^\Lambda)(T_{AA} - T_{AB})}{L_{AA}^\Lambda + L_{BB}^\Lambda + 2L_{AB}^\Lambda}\delta c_A \\ &- \frac{(L_{BB}^\Lambda + L_{AB}^\Lambda)(T_{BB} - T_{BA})}{L_{AA}^\Lambda + L_{BB}^\Lambda + 2L_{AB}^\Lambda}\delta c_A. \end{aligned} \tag{32}$$

The vacancy concentration field is then predicted to be sinusoidal, with a wavelength similar to the atomic one and a relative amplitude of the same order of the atomic one. The vacancy fluctuation results from a Kirkendall effect: the larger the difference between the diffusion coefficients of A and B [roughly equal to, respectively, the first and second numerator of Eq. (32)], the larger the fluctuation. If A is the most rapid species, the vacancy and species A concentration profiles are in phase, otherwise they are in antiphase.

In classical models for phase transformations, it is often assumed that a population of vacancy sinks and sources such as dislocations is efficient enough to guarantee a local equilibrium of vacancy. The deviation of the vacancy chemical potential from zero, $\delta\mu_V$, does not produce fluxes, since it is assumed that elimination and production of vacancy can be achieved locally. Fluxes of atoms and vacancies are induced by the atomic chemical potential gradients. From the Gibbs-Duheim relationship, $c_A\delta\mu_A + c_B\delta\mu_B + c_V\delta\mu_V = 0$, the local equilibrium status of vacancy ($\delta\mu_V = 0$), and the assumption that c_V is very small compared to c_A and c_B, we easily show that

$$-\frac{\delta\mu_A}{c_B} = \frac{\delta\mu_B}{c_A} = \delta(\mu_B - \mu_A) = \frac{\Phi^{\Lambda}_{\mathrm{CH}}}{\beta}\delta c_B, \tag{33}$$

where the relationship between the alloy chemical potential driving force and the discrete CH driving force is a direct consequence of the definition of the latter (cf. Appendix A). Inspection of Eq. (22) reveals that the rate equations of dc_A/dt and dc_B/dt are controlled by a single driving force, the alloy driving force $\nabla\beta\delta(\mu_B - \mu_A)$. Instead, the vacancy kinetics is controlled by two driving forces, the alloy driving force and the vacancy chemical potential excess $\beta\delta\mu_V$. The local variation of the lattice site number resulting from the local elimination or production of vacancies leads to a lattice motion with a Kirkendall speed equal to the vacancy flux J_V [1]. The referentials of the lattice and the laboratory are thus not equivalent anymore. In the laboratory, a Kirkendall speed correction $c_\alpha J_V$ has to be added to the lattice atomic flux of chemical species α, which is equivalent to adding $-c_\alpha\nabla J_V$ to the RHS of $d\delta c_\alpha(k)/dt$:

$$\left(\frac{d\delta c_\alpha}{dt}\right)_{\mathrm{lab}} = \frac{d\delta c_\alpha}{dt} - c_\alpha\nabla J_V, \tag{34}$$

∇J_V corresponds to the sum of A and B time derivatives detailed in Eq. (22):

$$\begin{aligned}\nabla J_V &= -\Lambda\left[\left(L^{\Lambda}_{AA} + L^{\Lambda}_{AB}\right)\beta\delta\mu_A + \left(L^{\Lambda}_{BB} + L^{\Lambda}_{AB}\right)\beta\delta\mu_B\right] \\ &= -\Lambda\left[c_A\left(L^{\Lambda}_{BB} + L^{\Lambda}_{AB}\right) - c_B\left(L^{\Lambda}_{AA} + L^{\Lambda}_{AB}\right)\right]\Phi^{\Lambda}_{\mathrm{CH}}\delta c_B,\end{aligned} \tag{35}$$

where chemical potentials have been expressed with respect to the CH driving force after Eq. (33). In Eq. (34), the replacement of ∇J_V by Eq. (35), combined with Eqs. (34) and (33) leads to a single rate equation for the atomic concentration field obeying the form of Eq. (23), with an effective mobility M related to the interdiffusion coefficient $\tilde{D}$:

$$M(\Lambda) = c_A c_B\left[c_B\left(\frac{L^{\Lambda}_{AA}}{c_A} - \frac{L^{\Lambda}_{AB}}{c_B}\right) + c_A\left(\frac{L^{\Lambda}_{BB}}{c_B} - \frac{L^{\Lambda}_{AB}}{c_A}\right)\right], \tag{36}$$

with $M(\Lambda = 0) = \tilde{D}/f''$. The L^{Λ}_{ij} coefficients are deduced from Eqs. (20) and (29) and the corresponding heterogeneous correlation coefficient is deduced from Eqs. (30) and (31).

In conclusion, whatever the behavior of the vacancy population, the atomic concentration fluctuation is governed by an exponential with a frequency proportional to a mobility multiplied by the discrete CH thermodynamic driving force and a heterogeneous correlation coefficient f_Λ, which is a nonlinear function of Λ. The difference in vacancy behaviors leads to a difference of mobilities and heterogeneous correlation coefficients, which increases with the ratio L_{AA}/L_{BB}. When L_{AA} is larger than L_{BB} and c_A and c_B are of the same order, the mobility in the case of a conservative vacancy is controlled by the slow species, $M \simeq L^{\Lambda}_{BB}$, while the interdiffusion related mobility is controlled by the rapid species, $M \simeq c_B^2 L^{\Lambda}_{AA}$. The mobility, the heterogeneous correlation coefficient, and subsequently the rate of fluctuation decay will then depend on the experimental protocol. In some cases, the vacancy can be assumed to be at local equilibrium, and in some cases not. Dislocations can usually be assumed to be perfect point defect sinks and sources, homogeneously distributed in the sample with a density of the order of μ^{-3}. The characteristic length of diffusion is then respectively the nanometer for the atoms and the micrometer for the vacancy leading to a ratio of characteristic times between vacancies and atoms equal to $c_V 10^6$. Since in most of the cases, the vacancy concentration is several orders of magnitude smaller than 10^{-6}, the characteristic time for vacancies to diffuse toward point defect sinks is negligible with respect to the atom characteristic time. A more relevant question is to know whether vacancies can be eliminated at point defect sinks by taking diffusion directions different from that associated with the local atomic chemical potential gradient. If this is not verified, the relaxation kinetics of a vacancy toward local equilibrium cannot be decoupled from the kinetics of the atomic concentration fields and vacancies cannot be assumed to be at local equilibrium. For example, nonpercolated nanoscale microstructures resulting from a two-phase decomposition restrict the possible elimination paths of vacancy to a set of two-phase crossing paths along which atomic chemical potential gradients are nonzero. In that case, the vacancy should be treated more like a conservative species whose deviation from local equilibrium slows down the kinetics of atoms. Then the more appropriate definition for the mobility is given by Eq. (26). Like in Ref. [43], a complete study of the coupling regime between the chemical species kinetics and the relaxation of the vacancies would have been possible.

E. Heterogeneous correlation coefficient

In order to estimate the importance of the heterogeneous correlation coefficient f_Λ introduced by the SCMF theory [Eq. (30)], we perform a Taylor series expansion of the coefficient with respect to the wave-vector discrete operator Λ. First-order and second-order terms are respectively identified as a composition gradient-correlation parameter and a Laplacian-correlation parameter. The former parameter is then compared to the composition gradient-energy parameter of the CH thermodynamic driving force.

It is easy to show that the deviation from one of the wave-vector heterogeneous correlation coefficients defined

in Eq. (30) is directly proportional to the square of the off-diagonal Onsager coefficient L_{AB}:

$$f_\Lambda - 1 = -\frac{1}{Mm_1} q_\Lambda (L_{AB})^2, \tag{37}$$

with $q_\Lambda = Q_\Lambda - Q_{\Lambda=0}$. The expressions of mobility M and m_1 depend on the behavior of the vacancy. In the case of a conservative vacancy, M is deduced from Eq. (26) and an approximation of m_1 at zero order in L_{AB} is deduced from Eqs. (20), (29), and (26):

$$m_1 = c_A c_B \left(L_{AA}^{(0)} + L_{BB}^{(0)}\right). \tag{38}$$

In the case of nonconservative vacancy, M is deduced from Eq. (36) and an approximation of m_1 at zero order in L_{AB} is deduced from Eqs. (20), (29), and (36):

$$m_1 = \frac{c_A c_B L_{AA}^{(0)} L_{BB}^{(0)}}{\left(c_A^2 L_{BB}^{(0)} + c_B^2 L_{AA}^{(0)}\right)^2} \frac{L_{AA}^{(0)} L_{BB}^{(0)}}{L_{AA}^{(0)} + L_{BB}^{(0)}}. \tag{39}$$

Therefore the effect of wave vector on the heterogeneous correlation coefficient increases with the kinetic correlations or equivalently with the off-diagonal Onsager coefficient L_{AB} of the reference homogeneous solid solution. The resulting effective interdiffusion coefficient is deduced from Eq. (31):

$$D(\Lambda) = M\left[1 - \frac{1}{m_1 M} q_\Lambda (L_{AB})^2\right] \Phi_{\mathrm{CH}}^\Lambda. \tag{40}$$

The effective interdiffusion coefficient can be approximated by a second-order expansion in Λ:

$$D(\Lambda) = M\beta\left[f'' + \left(\kappa_E + \kappa_C^1\right)\Lambda + \kappa_C^2 \Lambda^2\right]. \tag{41}$$

The expression of the so-called composition gradient-correlation parameter κ_C^1 reads

$$\kappa_C^1 = -f'' q_\Lambda^1 (L_{AB})^2/(m_1 M). \tag{42}$$

As composition Laplacian-correlation parameter is defined as well:

$$\kappa_C^2 = \kappa_C^1 \left(\frac{q_\Lambda^2}{q_\Lambda^1} + \frac{\kappa_E}{f''}\right), \tag{43}$$

where q_Λ^1 and q_Λ^2 are the coefficients of the Taylor expansion $q_\Lambda = q_\Lambda^1 \Lambda + q_\Lambda^2 \Lambda^2$.

Note that a CH-like formulation of the effective interdiffusion coefficient is regained when the composition gradient-correlation parameter κ_C^1 is neglected. While a gradient-energy term arises as soon as 1nn thermodynamic interactions are considered, the gradient-correlation term arises only if nonequilibrium effective interactions beyond 1nn are considered. Within a BW approximation, κ_E does not vary with temperature and composition (cf. Appendix A). It is positive for an alloy with a clustering tendency and negative for an alloy with an ordering tendency. Instead, the gradient-correlation parameter κ_C^1 is a complex function of temperature and composition and is systematically negative for a reference state chosen to be an equilibrium solid solution. Kinetic correlations are then expected to decrease the total effective gradient parameter and make it vary with temperature. Both features were observed in Cu-Au alloys although the deviations from the theoretical value were attributed to experimental inaccuracy [18].

Up to now, it was argued that nonlinearity of D against Λ was due to long-range thermodynamic interactions. Indeed, thermodynamic interactions beyond 1nn interactions involve new discrete operators in addition to Λ and produce some nonlinearities of the effective interdiffusion coefficient. The wave-vector dependent parameter Q_Λ entering the mobility [see Eqs. (26) and (29)] systematically leads to nonlinearities of D because it is not a linear function of Λ. Moreover, Q_Λ increases with Λ. As explained in Refs. [12,18], the nonlinearity of D against Λ due to thermodynamics should vary with the direction of the sinusoidal fluctuation, while the one due to kinetic correlations depending on Λ only should be isotropic in a cubic crystal. However, note that the correlation contribution to D against wave vector k is direction dependent as Λ against k is direction dependent [cf. Eq. (25)]. At high temperature, the alloy tends to an ideal solid solution and nonlinearities due to thermodynamics should vanish, while some nonlinearities due to kinetic correlations could remain.

Note that a plot of D versus Λ can be used to obtain a value of the combination of Onsager coefficients $(L_{AB})^2/(m_1 M)$ by measuring κ_C^1. In general, an estimation of the free energy second derivative f'' can be obtained from thermodynamic databases. In the case of an alloy for which interaction energies beyond 1nn can be neglected, both the gradient-kinetic parameter κ_C^1 and the gradient-energy parameter κ_E can be extracted from a nanoscale diffusion experiment. Indeed, the use of Eq. (41) to fit the effective interdiffusion coefficient leads to $D(\Lambda = 0)$, κ_E and κ_C^1. If elastic interactions induced by coherency strains were accounted for, the picture would be more complex. Indeed, these interactions, which are direction dependent [12], should interplay with the kinetic correlations and hence contribute to both linear and nonlinear variation of D with Λ. This coupling effect is expected to be non-negligible if the variation of coherency strain and the resulting variation of vacancy exchange frequency with respect to local composition is large.

IV. RESULTS

In order to validate the main results obtained with the SCMF diffusion theory, a systematic comparison between the SCMF predictions and the Monte Carlo simulations is performed. The model alloys introduced to highlight the theoretical advances are then compared to some real alloys.

A. Monte Carlo simulation

Starting from the same atomic jump frequency model, AKMC simulations based on a time residence algorithm are performed [44]. The periodic simulation box is a bcc lattice with a total number of sites equal to $N_s = 512^3/4$. Sites are occupied by either A or B atoms except one empty site representing a vacancy. Several model alloys are studied: ideal solid solutions with different values of attempt frequencies ν_A and ν_B and solid solutions with interactions equal to zero except V_{AB} such that the resulting ordering energy $W = V_{AB}$ is either positive or negative.

Initial state of every simulation is a 1D sinusoidal composition-modulated solid solution along a [100] direction of the bcc lattice with an amplitude $\delta c_B = 0.01$ and a

wavelength λ [associated with $\Lambda = -8(\cos \Pi a/\lambda - 1)$ after Eq. (25)]. At a given temperature, one performs a metropolis algorithm [45] with direct exchange between atoms A and B belonging to the same plane perpendicular to the 1D sinusoidal direction. This way, a stationary short-range order under the constraint of a 1D sinusoidal concentration modulation is reached. The solid solution is then annealed, the concentration fluctuation decaying and the system evolving towards its equilibrium state. The temperature T is chosen to be above the critical temperature T_c ($T_c \simeq 0.2|2ZW|/k_B$ [46]) so that the equilibrium state corresponds to a uniform solid solution. At a given time, the sinusoidal average amplitude δc_i of species i is obtained from the λ component of the Fourier transformed 1D-concentration field. As discussed in Sec. III D, the vacancy is not expected to be at local equilibrium. It is then not possible to apply the rescaling time procedure used to predict the kinetics of systems including a nonconservative vacancy from AKMC simulations performed at a fixed number of vacancies [47]. Therefore, in the following AKMC simulations, the vacancy is considered as a conservative species. One introduces a reduced time $\tau = t \times c_V \nu_B$, where t is the physical time measured in the AKMC simulation at a vacancy concentration equal to $c_V = 1/N_s$. Even though the simulation box contains a single vacancy, a vacancy 1D-concentration profile can be measured by calculating the relative time spent by the vacancy in each plane perpendicular to the 1D direction (details of the averaging procedure are given in Ref. [47]).

We present first a practical example of the procedure used to measure the interdiffusion coefficient D in AKMC simulations. It is observed in Fig. 3 that the atomic artificial concentration wave introduced at the initial time in an ideal solid solution with a jump frequency ratio $\nu_A/\nu_B = 10$ remains, the amplitude decaying with time. Although the equilibrium vacancy concentration of this ideal solid solution is uniform and does not depend on local concentration, the vacancy concentration profile measured between two successive times is close to a sinusoidal profile in antiphase with the profile of atoms B. This is in agreement with the SCMF theory [see Eq. (32) of Sec. III D]. Note that symmetry breaking of the vacancy concentration profile naturally occurs in a stochastic Monte Carlo method. In particular, an excess of vacancies in the A-rich regions is predicted because the jump frequency of atoms A is larger than the one of atoms B. The logarithm of the atomic and vacancy fluctuation amplitude plotted in Fig. 4 is observed to be linear with time. A good quantitative agreement between the SCMF results and the AKMC simulations is obtained over a large range of modulation wavelengths λ, both for vacancies and atoms. Note that although the vacancy concentration oscillations measured in AKMC simulations are not perfectly sinusoidal, an average in space achieved by a Fourier transform yields a temporal evolution of the average amplitude in good agreement with the SCMF predictions. The effective interdiffusion coefficient $D(t)$ plotted in Fig. 6 is extracted from a fit of the logarithm of $\delta c_B(t)$ versus time, assuming a linear behavior with a slope equal to $-\Lambda D$ [see Eq. (27)].

B. AKMC simulations versus SCMF theory

Before discussing numerical predictions of the interdiffusion coefficient, we briefly indicate the relationship of the SCMF diffusion equation to the microscopic CH model [16]. If the contribution of the heterogeneous correlation coefficient to the general driving force is neglected [which is equivalent to put $\kappa_C^1 = 0$ in Eq. (41)], the SCMF equation becomes equivalent to a CH equation. The interdiffusion coefficients D obtained from the SCMF theory, the CH model, and the AKMC simulations are compared, first in an ideal solid solution then in interacting alloys.

In ideal solid solutions, the jump rate $W_{iV} = \nu_i$ is independent of the environment of the jumping atom i. Every configuration of atoms on the lattice sites has the same energy so that the distribution of atoms is random at thermodynamic equilibrium and the BW statistical mean-field approximation becomes exact. In that case, the discrepancies of the SCMF results are only due to the truncation of the effective Hamiltonian used to calculate the kinetic correlations. The convergence of the diffusion coefficient D against the kinetic

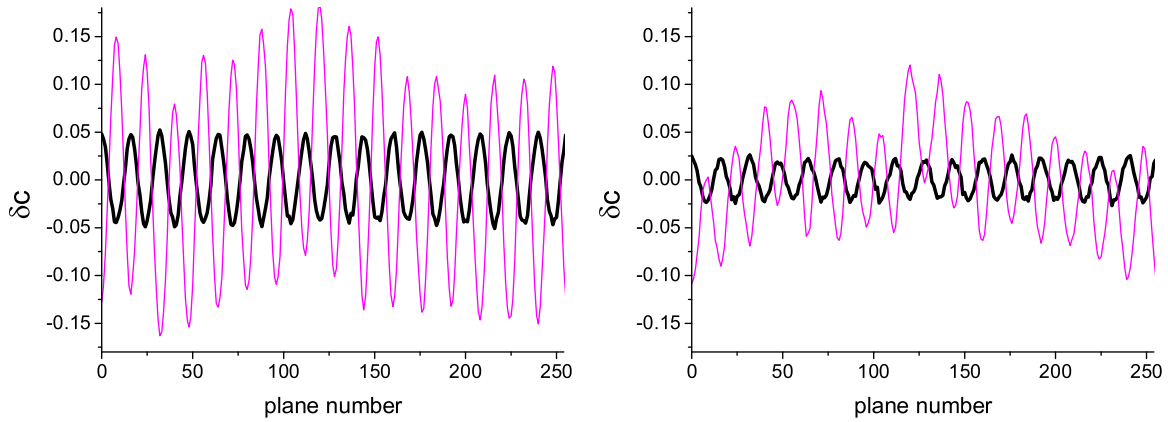

FIG. 3. (Color online) Temporal evolution of concentration profiles started from an initial sinusoidal concentration profile of solute B with wavelength equal to $16(a/2)$ and amplitude equal to 0.01, and a single vacancy in the simulation box. Profiles are plotted against plane numbers along the [100] direction with a distance $d = a/2$ between planes. They are extracted from AKMC simulations of a noninteracting alloy AB at composition $c_B = 0.9$ with an exchange frequency ratio $\nu_A/\nu_B = 10$, at two successive reduced times, $\tau_1 = 0.6$ (left) and $\tau_2 = 1.2$ (right) in dimensionless units ($c_V \nu_B t$). $\delta c_V/c_V$ is represented by a magenta thin line and δc_B by a black thick line.

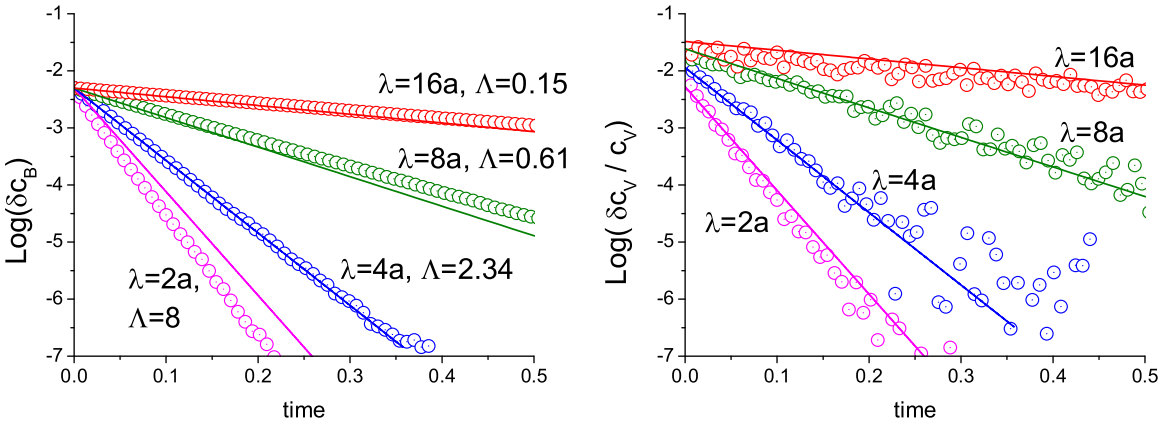

FIG. 4. (Color online) Temporal variation of the logarithm of the maximum of the sinusoidal concentration field associated with solute atoms (left) and a vacancy for which $\delta c_V/c_V$ is represented (right). Circles represent the AKMC simulations and solid lines the SCMF predictions for a noninteracting alloy AB at composition $c_B = 0.9$ with an exchange frequency ratio $\nu_A/\nu_B = 10$ and various wavelengths λ expressed in units of lattice parameter a. The corresponding values of the wave-vector discrete operator Λ are indicated on the left figure. Time is in dimensionless units ($c_V \nu_B t$).

approximation is illustrated in Fig. 5 for an ideal solid solution of atoms A and tracer atoms $B = A^*$ with the same jump frequencies and in Fig. 6 for an ideal solid solution with a large jump frequency ratio $\nu_A/\nu_B = 10$. Note that in AA^* solutions, the interdiffusion coefficient D does not depend on the nominal composition of atoms A^*, thereby the Λ variation of the resulting diffusion coefficient is totally determined by the crystal geometry. Instead, in the AB solid solution with $\nu_A = 10\nu_B$, D strongly depends on c_B. The convergence study is chosen to be presented for $c_B = 0.9$, a composition at which the kinetic properties of the alloy are strongly affected by the kinetic correlations. As a general trend, a (1nn)-shell approximation of the SCMF theory completely fails to predict the variation of D against Λ. As explained in Sec. III, the latter approximation does not produce gradient-correlation parameters κ_C^1. Moreover, the gradient-energy parameter κ_E is null in ideal solutions, explaining the constant value of D against wave vector. When Λ is very small, the convergence of D is mainly controlled by the convergence of the Onsager phenomenological coefficients L_{ij}. In the AA^* solution, at $\Lambda < 5$, the convergence is achieved with a $(1nn)^3$ kinetic shell approximation, in agreement with what is observed for the self-diffusion correlation factor studied in Ref. [27]. In the large jump-frequency ratio solid solution, at $\Lambda \simeq 0.15$ (corresponding to $\lambda = 16a$), we observe in Fig. 6 that the present SCMF calculation of D does not converge toward the AKMC value, although the $(1nn)^2$ and $(1nn)^3$ values are very close to each other. A previous study of model alloys with large jump-frequency ratios, demonstrated that an effective Hamiltonian limited to pair interactions is not adequate for an accurate estimation of the L_{ij} [29], hence explaining the discrepancy of the present pair effective SCMF calculation at small Λ.

In the AA^* solution at $\Lambda > 5$, the decrease of D against Λ is underestimated by the $(1nn)^2$ approximation and overestimated by the $(1nn)^3$ approximation as illustrated by Fig. 5. Moreover, the large difference observed between the $(1nn)^2$

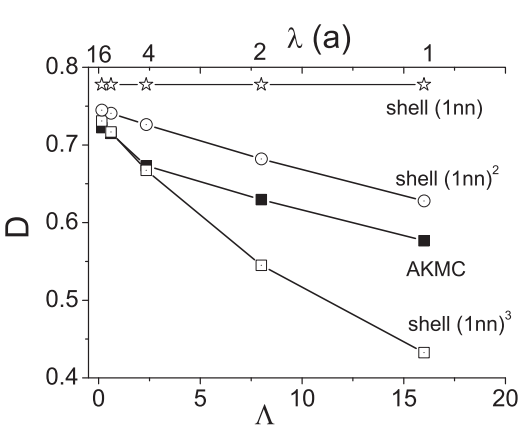

FIG. 5. Diffusion coefficient in dimensionless units $[D/(c_V\nu_B)]$ with respect to wave-vector operator Λ (the corresponding wavelength λ in units of lattice parameter a is indicated on the top axis), measured in the AKMC simulations (filled symbols) and predicted by successive kinetic SCMF approximations for a noninteracting alloy with $\nu_A = \nu_B$.

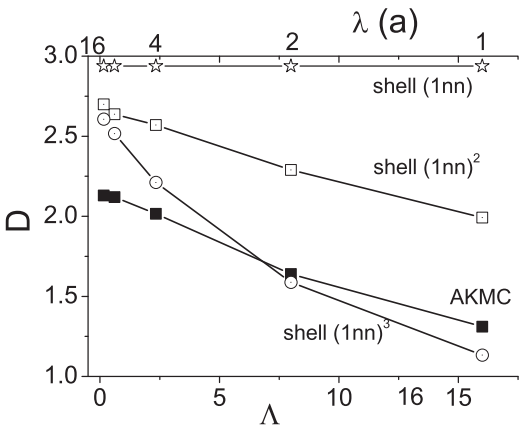

FIG. 6. Diffusion coefficient in dimensionless units $[D/(c_V\nu_B)]$ with respect to wave-vector operator Λ (the corresponding wavelength λ in unit of lattice parameter a is indicated on the top axis), measured in the AKMC simulations (filled symbols) and predicted by successive kinetic SCMF approximations for a noninteracting alloy with $\nu_A = 10\nu_B$ at composition $c_B = 0.9$.

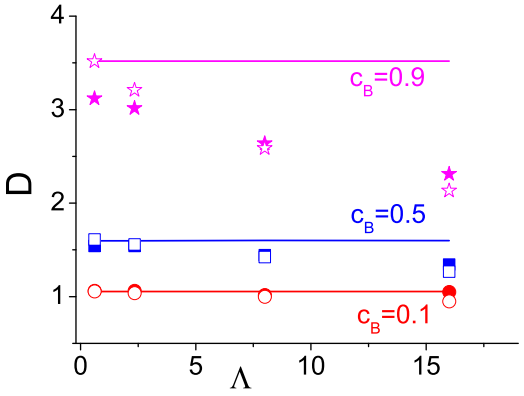

FIG. 7. (Color online) Interdiffusion coefficient in dimensionless units $[D/(c_V v_B)]$ with respect to wave-vector operator Λ measured in AKMC simulations (filled symbols) and predicted by SCMF predictions (empty symbols) for a noninteracting alloy with $v_A/v_B = 10$ and at various nominal compositions c_B. For the sake of clarity, 1 has been added to the values associated with $c_B = 0.9$. Lines represent the results of the CH like model.

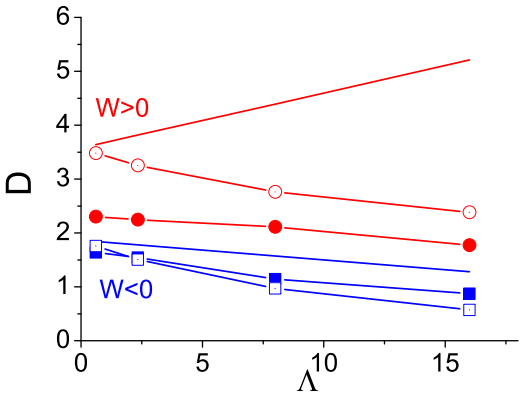

FIG. 9. (Color online) Interdiffusion coefficient in dimensionless units $[D/(c_V v_B)]$ with respect to wave-vector operator Λ measured in AKMC simulations (filled symbols) and predicted by SCMF for alloys with a clustering tendency ($W > 0$, circles) and an ordering tendency ($W < 0$, squares), $v_A = 10v_B$, at $T/T_c = 2.4$ and $c_B = 0.9$.

and $(1nn)^3$ approximations prompts us to think that the convergence of the pair-effective SCMF calculation is not achieved yet. If longer range effective pair interactions than the ones included in the $(1nn)^3$ were considered, we could expect a better agreement with the AKMC simulations. Surprisingly, in the ideal solution with a large jump-frequency ratio, a good agreement is observed between the $(1nn)^3$ SCMF predictions and the AKMC results at $\Lambda > 1$ (cf. Fig. 6). It seems that when there is a strong interaction between kinetic correlations and the modulation wavelength, the convergence of the SCMF results with respect to the kinetic shell approximation is more rapid.

Note that the present CH model is almost similar to the (1nn)-shell approximations presented in Figs. 5 and 6. In the former, a $(1nn)^3$-shell approximation is used to calculate mobility M as opposed to the (1nn) approximation of M used in the latter. In what follows, we systematically compare the results of the CH model, the SCMF theory within the highest $(1nn)^3$ kinetic shell approximation and the AKMC simulations. A way to estimate the kinetic correlation contribution is to measure the difference between the CH and SCMF plots.

In Fig. 7, the interdiffusion coefficient is plotted for three nominal compositions of the ideal solution AB with $v_A/v_B = 10$. As expected, the CH model fails in describing the variation of D against Λ. However, in the dilute alloy $A(B)$, the mismatch between the CH and AKMC results is very small, indicating that the Λ variation of the kinetic correlations is negligible. As explained in Sec. III E, this variation is related to the off-diagonal Onsager coefficient, which is smaller in dilute alloys $[L_{AB}/(v_B c_V) = 0.033$ at $c_B = 0.1]$ than in concentrated alloys $[L_{AB}/(v_B c_V) = 0.062$ at $c_B = 0.9]$. When wavelength distances reach 1–2 lattice parameters, D becomes nonlinear with Λ, a feature which is well reproduced by the SCMF theory. It is demonstrated here, that a nonlinear behavior of D may occur in systems with short range thermodynamic interactions, due to kinetic correlations.

In an interacting alloy, the ensemble averages calculated by means of the BW approximation are not exact anymore. Then both the kinetic correlations and the thermodynamic averages are approximated. Nevertheless, an examination of Figs. 8 and 9 demonstrates that a qualitative and semiquantitative agreement with the AKMC results is obtained. The predicted sign of the Λ variation of D is systematically the right one. For instance, in solid solutions with a clustering tendency, due to the positive gradient-energy parameter κ_E, an increase of D against Λ is expected as shown by the CH plot, while

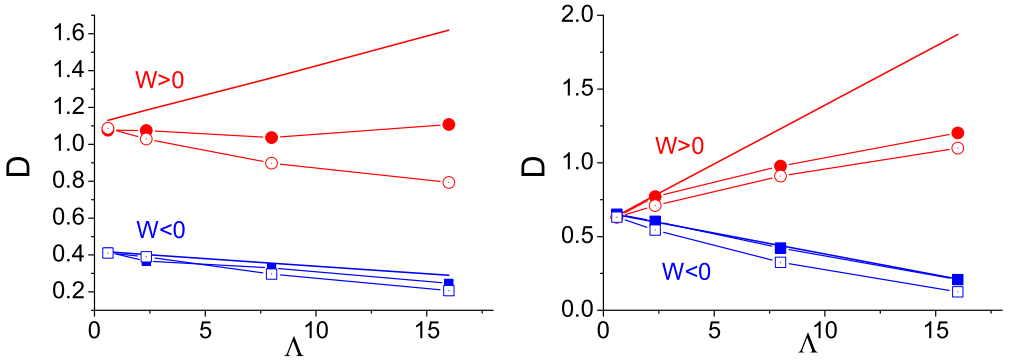

FIG. 8. (Color online) Interdiffusion coefficient in dimensionless units $[D/(c_V v_B)]$ with respect to wave-vector operator Λ measured in AKMC simulations (filled symbols) and predicted by successive kinetic SCMF approximations for a alloys with a clustering tendency ($W > 0$) and an ordering tendency ($W < 0$), $v_A = v_B$, at $T/T_c = 2.4$ and $c_B = 0.1$ (left), and $c_B = 0.5$ (right).

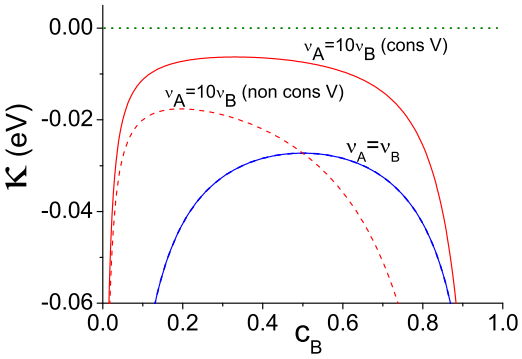

FIG. 10. (Color online) Composition gradient-energy and gradient-correlation parameters in eV, κ_E (green dotted line), and κ_C^1 (dashed and solid lines), with respect to the nominal composition in a noninteracting alloy for two different ratios of attempt frequencies $\nu_A = 10\nu_B$ and ν_B. Dashed (respectively, solid) lines are for a nonconservative (respectively, conservative) treatment of the vacancy.

both AKMC and SCMF results exhibit a negative variation of D. The latter is observed when the negative gradient-kinetic parameter is dominant over the gradient-energy parameter. Therefore a negative slope of the effective interdiffusion coefficient against Λ does not imply an ordering tendency of the alloy. This statement should modify the analysis of previous nanoscale diffusion experiments. For instance, a negative composition gradient parameter is measured in Cu-Ni alloys, while these alloys are known to have a clustering tendency [19]. It is worth noticing that a spinodal decomposition theory relying on the present SCMF diffusion equation would predict new kinetic behaviors. A nonstable solid solution with a negative second derivative of the free energy f'' and a dominant gradient-correlation parameter over the gradient-energy parameter, would exhibit a negative D at any wavelength and an associated structure factor with no peak, monotonously decreasing from the shortest to the largest wavelength [6]. As a general trend, the kinetic correlations are expected to shift the peak position of the structure factor toward smaller wavelengths.

In alloys with an ordering tendency, plots of D in Fig. 8 are observed to be less affected by the kinetic correlations because the CH results are very close to the AKMC values. However, when the attempt frequency ν_A is different from ν_B, a kinetic correlation effect appears in Fig. 9.

Note that the AKMC simulations by themselves bring significant conclusions. Indeed, the simulations of noninteracting or interacting alloys associated with the same ordering energy and different attempt frequency ratios show a different variation of the effective interdiffusion coefficient. This is a proof that the variation of D is affected by the kinetic parameters at variance with the usual statement of the phenomenological kinetic models.

C. SCMF predictions

Now that the SCMF theory has been validated against the AKMC simulations, we use it to predict general behaviors of the composition Laplacian parameter κ_C^2 and gradient parameter decomposed into gradient-energy κ_E and gradient-correlation κ_C^1 parameters. These parameters plotted against the nominal composition provide with an indication of their relative contribution to the variation of the diffusion coefficient D against Λ. The results obtained with a nonconservative and conservative treatment of vacancies are systematically compared.

The first three figures illustrate the variation of the gradient energy parameters with respect to the nominal composition at two temperatures and two attempt frequency ratios, in ideal alloys (Fig. 10), clustering alloys (Fig. 11), and ordering alloys (Fig. 12). As a general trend, κ_E remains constant against c_B and temperature, κ_C^1 is dominant at small compositions of A or B, and the nonconservative treatment of the vacancy leads to larger gradient-correlation parameters than the ones associated with the conservative vacancy. In alloys with equal attempt frequencies, gradient parameters are symmetric. A ratio ν_A/ν_B larger than one increases the contribution of the gradient-correlation parameter at a large solute concentration c_B and decreases the same contribution at a small c_B. In interacting alloys, the relative contribution of κ_C^1 to the total composition gradient parameter increases with temperature. In clustering alloys, the kinetic correlation effect is more pronounced and affects a larger composition range of the alloy. The change of sign of κ_C^1 occurring at $T/T_c = 0.8$ is due to the change of sign of the second derivative of the free energy f''. Between both spinodes associated with $\kappa_C^1 = 0$, f'' is

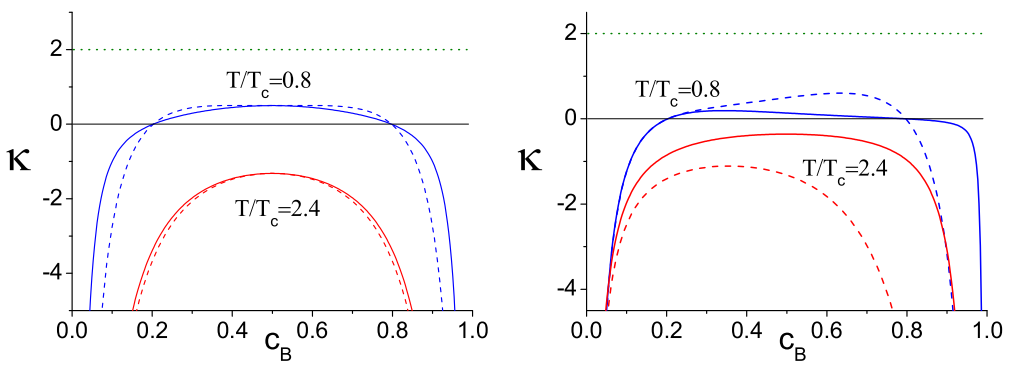

FIG. 11. (Color online) Gradient-energy and gradient-correlation parameters in reduced units [κ_E/W (green dotted line) and κ_C^1/W (dashed and solid lines)], with respect to the nominal composition in an alloy with a clustering tendency ($W > 0$) at two temperatures $T/T_c = 2.4$ and 0.8. Attempt frequencies are equal (left) and $\nu_A = 10\nu_B$ (right). Dashed (respectively, solid) lines are for a nonconservative (respectively, conservative) treatment of the vacancy.

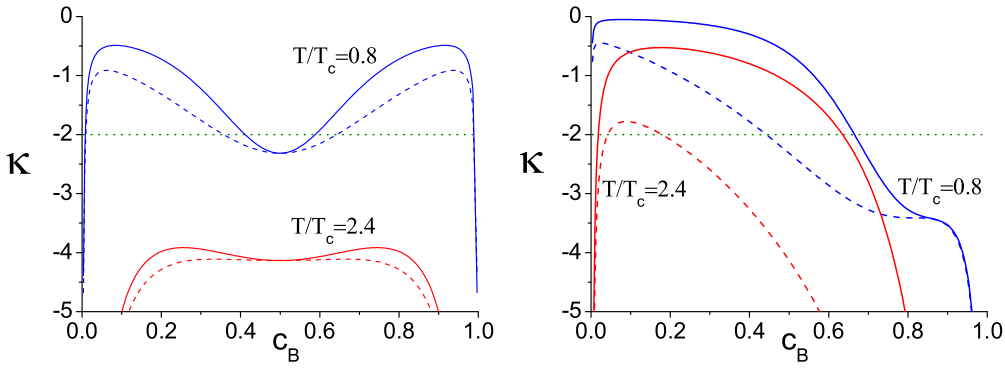

FIG. 12. (Color online) Gradient-energy and gradient-correlation parameters in reduced units $[\kappa_E/(-W)$ (green dotted line) and $\kappa_C^1/(-W)$ (dashed and solid lines)], with respect to the nominal composition in an alloy with an ordering tendency ($W < 0$) at two temperatures $T/T_c = 2.4$ and 0.8. Attempt frequencies are equal (left) and $\nu_A = 10\nu_B$ (right). Dashed (respectively, solid) lines are for a nonconservative (respectively, conservative) treatment of the vacancy.

negative and the solid solution is unstable. Within a classical spinodal decomposition theory, the corresponding gradient energy parameters determine the kinetics of fluctuation decay at wave vectors larger than a critical value k_c and of fluctuation growth at wave vectors smaller than k_c. As long as the attempt frequencies are equal and the homo-atomic interactions are equal, the contribution of the gradient-correlation parameter is small compared to the gradient-energy parameter.

The gradient parameters divided by f'' provide a quantitative estimation of the relative variation of D with respect to its value at zero wave vector [as shown in Eq. (41)]. Therefore the latter are plotted in the last three figures (Figs. 13–15). In addition to the gradient parameters, the Laplacian correlation parameters κ_C^2 are plotted. As a general trend, we observe that κ_C^2 has the same kind of variation against Λ as the corresponding gradient parameter κ_C^1. Its magnitude is roughly one order of magnitude below except inside the spinodal as shown in Fig. 14. However, when the wave vector Λ is larger than 10 (equivalent to have $\lambda < 2a$), the contribution $\kappa_C^2\Lambda$ is greater than κ_C^1 and a nonlinear variation of D appears. It is interesting to note that inside the spinodal as displayed by

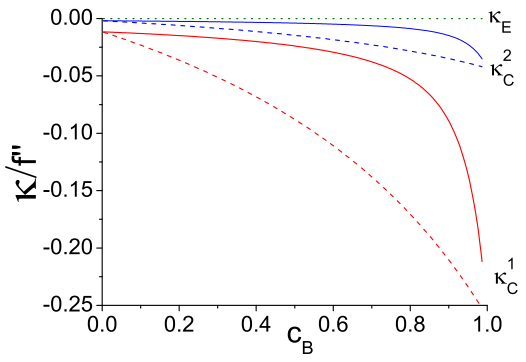

FIG. 13. (Color online) Composition gradient and Laplacian parameters divided by the second derivative of the free energy f'', κ_E/f'' (dotted green line), κ_C^1/f'' (dashed and solid red lines), and κ_C^2/f'' (dashed and solid blue lines) with respect to the nominal composition in a noninteracting alloy for the attempt frequency ratio $\nu_A = 10\nu_B$. Dashed (respectively, solid) lines are for a nonconservative (respectively, conservative) treatment of the vacancy.

Fig. 14, while κ_C^1 is small with respect to κ_E, the contribution of $\kappa_C^2\Lambda$ to the coefficient D and the rate of phase decomposition is expected to be at least as important as κ_E. The single κ_C^2 parameter induces a decrease of around 40% of the diffusion coefficient in the alloy at $\Lambda = 10$. Part of the strong linearity of D measured in most of the alloys during a spinodal phase decomposition might be due to these kinetic correlation effects [48].

In the clustering solid solution represented in Fig. 14 at $T/T_c = 2.4$, the maximum of the relative variation of D is roughly 15% due to κ_E and −20% due to $\kappa_C^1 + \Lambda\kappa_C^2$ at $\Lambda = 10$. In Fig. 15, displaying ordering alloys, D is less affected by the composition gradient parameters. At both $T/T_c = 2.4$ and 0.8 the relative variation of D due to κ_C^1 reaches a maximum of 9% and is around the same for κ_C^2 at $\Lambda = 10$. The total relative variation of D at $T/T_c = 2.4$ in both the clustering and ordering alloys can also be measured in Fig. 8.

D. Model alloys versus real alloys

Experimentally, the kinetic properties of concentrated solid solutions AB are mainly characterized by the tracer diffusion coefficients D_A^* and D_B^* [49]. Within the BW approximation of the SCMF theory, the tracer diffusion ratio D_A^*/D_B^* like the heterogeneous correlation coefficient (see Ref. [27] and Eq. (30)), depend on a unique kinetic parameter, the ratio of the average exchange frequencies, $L_{AA}^{(0)}/L_{BB}^{(0)}$. The tracer diffusion ratio is thus chosen to be a kinetic signature and it is used for the comparison between the model and real alloys. The theoretical tracer diffusion ratios plotted against the alloy composition in Fig. 16 are deduced from the SCMF theory within the same BW approximation (the analytical formulas are presented in Ref. [27]). The experimental tracer diffusion data are mainly obtained from a diffusion database [49] in which for a few binary systems tracer diffusivities of both elements are available. The phase diagrams are then used to get a thermodynamic characterization of the solid solutions. An estimation of the sign of the ordering energy W is obtained from the phase diagram: a solid solution which at lower temperature is separated in two phases is associated with a clustering tendency ($W > 0$), instead a solid solution that forms an ordered phase at a lower temperature is associated

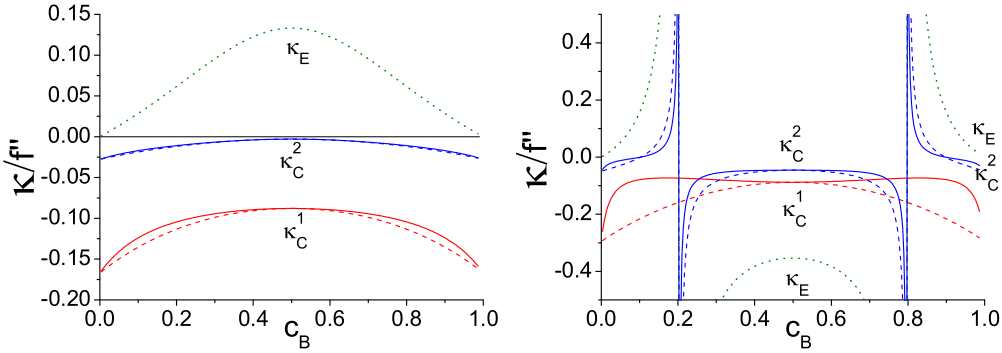

FIG. 14. (Color online) Composition gradient and Laplacian parameters divided by the second derivative of the free energy f'', κ_E/f'' (dotted green line), κ_C^1/f'' (dashed and solid red lines), and κ_C^2/f'' (dashed and solid blue lines) with respect to nominal composition in a clustering alloy ($W > 0$) with equal attempt frequencies, at $T/T_c = 2.4$ (left) and 0.8 (right). Dashed (respectively, solid) lines are for a nonconservative (respectively, conservative) treatment of the vacancy. Divergence of κ_E/f'' and κ_C^2/f'' is occurring at the spinodal line (compositions at which $f'' = 0$) and plots inside the spinodal are for unstable solid solutions.

with an ordering tendency ($W < 0$). A rough estimation of the critical temperature T_c is extracted as well.

In the case of a clustering tendency ($W > 0$), three examples of well characterized bcc solid solutions have been found. The first example is the concentrated paramagnetic Fe-Cr solid solution. The diffusion experiments performed at temperatures above 1100 K $\simeq 1.2T_c$ show that the Fe and Cr tracer diffusion coefficients are very close, with Cr diffusing slightly faster than Fe [49,50]. The Fe-Cr system is then not so far from the clustering model alloy with equal attempt frequencies $\nu_A = \nu_B$ leading to a tracer diffusion ratio close to one (see the right figure in Fig. 16). Instead, the tracer diffusion ratio associated with the solid solution Ti-V is large: $D^*_{\mathrm{Ti}}/D^*_{\mathrm{V}} \simeq 5$ at $T = 1500$ K $\simeq 2T_c$ and $c_V = 0.9$ [49]. This system is closer to the clustering model alloy with a large attempt frequency ratio $\nu_A = 10\nu_B$ leading to a tracer diffusion ratio around 6 at $c_B = 0.9$ (see the left figure in Fig. 16 at $c_B = 0.9$). The system Nb-Ti in which $D^*_{\mathrm{Ti}} = 2 - 3D^*_{\mathrm{Nb}}$ at $c_{\mathrm{Ti}} = 0.64$–0.80 and $T = 1250$–1400 K, and $T_c = 800$ K, is between both clustering model alloys. The ordering model alloy with equal attempt frequencies, leading to a tracer diffusion ratio very close to one should be a good representative of the system Fe-Ni (see the right figure in Fig. 16). Indeed, in Fe-Ni, the tracer of Fe is slightly faster than the Ni one at temperatures around $T \simeq 1300$ K $\simeq 1.8T_c$ [49].

To conclude, the main correlation effects analyzed in the previous section should happen in these real alloys. In particular, a change of sign of the composition gradient parameter and strong nonlinearities of the interdiffusion against Λ are expected in Ti-V (see the right figure in Fig. 11).

Some measurements of nanoscale diffusion coefficients have been performed in face centered cubic solid solutions by using x-ray diffraction on crystalline metals deposited in epitaxial layers with wavelengths below a few nanometers [5]. Composition gradient effects are systematically observed. Although the present diffusion theory is applied to bcc alloys, the same behavior is expected for fcc alloys. For this reason, some of the available nanoscale interdiffusion coefficients are analyzed within the framework of the SCMF theory. Mainly one system was observed to behave as predicted by a CH-like model: the ordering Ag-Au alloy at temperatures $T = 460$–550 K and compositions $c_{\mathrm{Au}} = 18$–27 at.% [16]. The measured composition gradient effects could be explained by an elastic energy model combined with a regular solution model of κ_E, and it was found to be fairly independent of temperature and composition, as expected from the regular solution model. In this system, the tracer diffusion ratio is

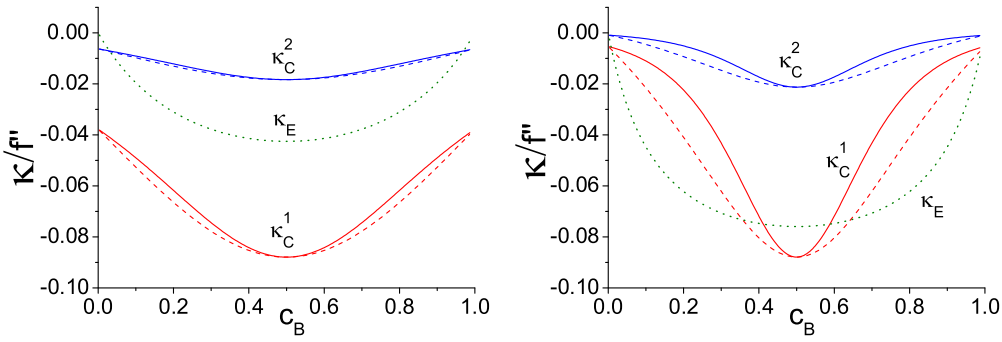

FIG. 15. (Color online) Composition gradient and Laplacian parameters divided by the second derivative of the free energy f'', κ_E/f'' (dotted green line), κ_C^1/f'' (dashed and solid red lines), and κ_C^2/f'' (dashed and solid blue lines) with respect to the nominal composition in an ordering alloy ($W < 0$) with equal attempt frequencies, at $T/T_c = 2.4$ (left) and 0.8 (right). Dashed (respectively, solid) lines are for a nonconservative (respectively, conservative) treatment of the vacancy.

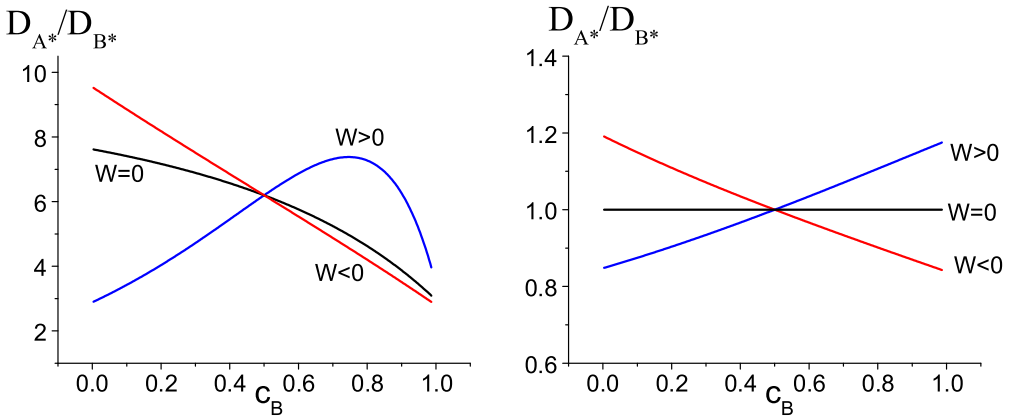

FIG. 16. (Color online) Ratio of tracer diffusion coefficients against the alloy composition at $T/T_c = 2.4$, with (left) $\nu_A = 10\nu_B$ and (right) $\nu_A = \nu_B$ for a clustering alloy ($W > 0$), an ordering alloy ($W < 0$) and an ideal solid solution $W = 0$. The values are predicted by the SCMF theory [27].

$D^*_{\rm Ag}/D^*_{\rm Au} = 3$ for $c_{\rm Au} < 0.25$ and the critical temperature is $T_c \simeq 160$ K. A comparison with the ordering model alloy with $\nu_A = 10\nu_B$ leading to a slightly larger tracer diffusion ratio (see the left figure in Fig. 16) shows that a SCMF prediction for this system would lead to a non-negligible contribution of kinetic correlations and a resulting composition gradient parameter different from a CH prediction (see the right figure in Fig. 12 at $c_B < 0.3$). Moreover, the correlation contribution should vary with temperature and composition. However, it is interesting to note that a conservative treatment of vacancy leads to a very different kinetic behavior: the composition gradient-correlation parameter becomes negligible over a large range of composition and temperature. Although, the interaction model and the present SCMF approximations should be improved to get a clear conclusion on this system, the role of sinks and sources in the elimination and production of vacancy in this system should be studied in details as well.

As already mentioned, the alloy Ni-Cu was recognized to be a system departing from a CH model [19]. Indeed, although a positive composition gradient parameter was expected for this clustering system, the effective composition gradient measured in Ni- 50 at.% Cu at $T = 675$ K $\simeq 1.1T_c$ was observed to be negative. An introduction of long-range interactions into the calculation of the composition-gradient energy parameter could explain the change of sign, but the predicted amplitude was an order of magnitude below the experimental value. The tracer diffusion ratio measured at $T = 1133$ K $\simeq 1.9T_c$ is around 3 on the whole composition range of Cu which is a little smaller than what is obtained for a clustering model alloy and jump frequency ratio equal to 10 (see the left figure in Fig. 16). For this kind of diffusivity behavior, the SCMF theory predicts an important contribution of the heterogeneous kinetic correlations, which potentially may change the sign of the effective composition gradient parameter (see the right figure in Fig. 11).

Another interesting example is the ordering alloy Cu-16 at.% Au [18]. A calculation based on the regular solution model combined with an elastic model leads to a value in fairly good agreement with the measured gradient parameter. However, the observation of an increase of the composition gradient between $T = 400$ and 435 K is in contradiction with the temperature free composition gradient-energy parameter predicted by the regular solution model. In Cu-Au, the tracer diffusion ratio is roughly equal to $D^*_{\rm Cu}/D^*_{\rm Au} \simeq 1.5$ at $c_{\rm Au} = 0.1$–0.3 and at $T = 1133$ K $= 1.6T_c$, a value which is comparable to what is obtained in the ordering model alloy with equal attempt frequencies (see the right figure in Fig. 16). For this type of alloy, the SCMF theory predicts a strong variation of the composition gradient-correlation parameter with respect to temperature (see the left figure in Fig. 12 at $c_B < 0.3$). To conclude, some of the qualitative features of the heterogeneous correlation effects seem to be in agreement with the kinetic behavior of a few fcc multilayer alloys characterized at the nanoscale, for example, the negative composition gradient parameter κ observed in some clustering alloys, the variation of κ against temperature and composition and the nonlinearities of D at short wavelengths ($\simeq$1–2 nm).

V. CONCLUSION

Atomic kinetic equations of the concentration fields in a nonuniform gradient of chemical potential are derived from the SCMF theory. The phenomenological TIP equations are obtained as a limit of the atomic equations when wave vector is tending to zero (i.e. when chemical potential gradients are uniform). At finite wave vector, general driving forces including deviations of the free energy from a local equilibrium thermodynamic formulation have to be defined. These deviations are related to the variation of vacancy motion due to the spatial variation of the alloy composition. During the characteristic time of atomic diffusion, multiple exchanges of the vacancy with the same atoms may happen, inducing atomic kinetic correlations, which depend as well on the spatial variation of the alloy composition. The AKMC simulations of model alloys associated with the same thermodynamic parameters and different attempt frequencies yield different variation of D against Λ proving that a model of composition gradient parameter defined in terms of thermodynamic constants only is not valid. The effect of wave vector on the kinetic correlations can be larger than the composition-gradient

energy contribution. In demixting alloys with large kinetic correlations, the corresponding gradient-correlation parameter may change the sign of the total composition gradient parameter. A clear indication of the importance of the kinetic correlations is the nonlinear behavior of the AKMC diffusion coefficient at large wave vector, which is not predicted by the CH model. The SCMF theory within a BW statistical approximation and a third-shell ($1nn^3$) kinetic approximation is shown to be able to reproduce the change of sign of the total composition gradient parameter, the nonlinear behavior of the effective interdiffusion coefficient, and yields diffusion coefficient values in semiquantitative agreement with the AKMC values.

A particular striking feature of the present theory is to show that in addition to the thermodynamic driving force such as the one defined by Cahn-Hilliard, a heterogeneous correlation coefficient should be considered. The latter includes a gradient-kinetic parameter as well as nonlinear kinetic contributions. The resulting effective interdiffusion coefficients D are predicted to be lowered by the kinetic correlations. Although the analysis of kinetic correlations is performed on model alloys, the values of the key kinetic and thermodynamic parameters are demonstrated to be close to the ones of some real bcc binary alloys. Therefore the heterogeneous kinetic correlation effects highlighted here should happen in real alloys.

The same theory can be combined with better statistical approximations. An extension of the SCMF theory to multicomponent alloys and other diffusion mechanisms should yield the same qualitative features. Indeed, the kinetics of pair probabilities is independent from the one of the concentration field as soon as nonequivalent transition frequencies are available to exit a pair configuration. The deviations of the asymmetric pair probabilities from local equilibrium values represent the kinetic correlations, while the deviations of the symmetric pair probabilities from local equilibrium values represent the thermal fluctuations of the concentration field. Therefore a deterministic approach such as the SCMF mean-field theory should then be able to include the effects of thermal fluctuations on a spinodal decomposition kinetics.

ACKNOWLEDGMENTS

We want to thank Frédéric Soisson, Bernard Legrand, and Georges Martin for fruitful discussions and technical support. This work also contributes to the Joint Programme on Nuclear Materials (JPNM) of the European Energy Research Alliance (EERA).

APPENDIX A: DRIVING FORCES

Within the Bragg-Williams approximation, the expression of the chemical potential difference corresponds to the solution of the regular solid solution:

$$\beta\mu_i^{AV} = \ln\frac{c_i^A}{c_i^v} + \sum_{s,\zeta}\delta_{is}\zeta(V_{A\zeta} - V_{V\zeta})c_s^\zeta. \tag{A1}$$

The resulting expression of $T_{\alpha\zeta}(k)$ defined in Eq. (21) is then

$$T_{\alpha\zeta} = \beta\frac{\partial\mu_{\alpha V}}{\partial c_\zeta} + \Lambda(k)\beta(V_{\alpha\zeta} - V_{V\alpha}) \tag{A2}$$

and

$$\beta\frac{\partial\mu_{\alpha V}}{\partial c_\zeta} = \delta_{\alpha\zeta}^{Kr}\frac{1}{c_\alpha} + \frac{1}{c_V} + Z\beta(V_{\alpha\zeta} - V_{\alpha V}), \tag{A3}$$

where $\delta_{\alpha\zeta}$ is equal to 1 if $\alpha = \zeta$ and 0 if else.

The CH driving force $\Phi_{\mathrm{CH}}^{\Lambda}$ is defined as the second derivative of the binary alloy AB free energy with respect to the solute concentration c_B. In the reciprocal space, it is given by

$$\Phi_{\mathrm{CH}}^{\Lambda} = \beta f'' + \Lambda(k)\beta\kappa. \tag{A4}$$

f'' corresponds to the first derivative of the alloy chemical potential $\mu_{AB} = \mu_A - \mu_B$ with respect to c_B,

$$\beta f'' = \beta\frac{\partial\mu_{AB}}{\partial c_B} = \frac{1}{c_A c_B} - 2Z\beta W, \tag{A5}$$

and κ_E is the gradient-energy parameter

$$\kappa_E = 2W. \tag{A6}$$

W is the ordering energy which is equal to $W = -0.5(V_{AA} + V_{BB} - 2V_{AB})$ and Z is the number of 1nn sites.

Note that some combinations of the coefficients of the T matrix lead to expressions corresponding to $\Phi_{\mathrm{CH}}^{\Lambda}$ at zero order in c_V:

$$\Phi_{\mathrm{CH}}^{\Lambda} = c_V(T_{AA}T_{BB} - T_{AB}T_{BA}) = T_{AA} + T_{BB} - 2T_{AB}. \tag{A7}$$

APPENDIX B: KINETIC EQUATIONS OF THE PAIR CORRELATORS

Along the [100] direction, pair correlators considered in the 1nn1nn shell are grouped together in the vector $U_i = (A_{i,1}^{AV}, S_{i,1}^{AV}, A_{i,2}^{AV}, S_{i,2}, P_{i,2}, A_{i,3}^{AV}, S_{i,3}, P_{i,3}, A_{i,5}^{AV}, S_{i,5})$. Within the 1nn1nn1nn shell, pair correlators are the ones of the 1nn1nn shell plus the first nn of the 1nn1nn sites, leading to four 4th nn effective interactions $(A_{i,4a}^{AV}, S_{i,4a}, A_{i,4b}^{AV}, S_{i,4b})$, four 7th nn effective interactions $(A_{i,7a}^{AV}, S_{i,7a}, A_{i,7b}^{AV}, S_{i,7b})$, and two 10th effective interactions $(A_{i,10}^{AV}, S_{i,10})$. The whole set of pair correlators are grouped together in the vector U_i and ordered by their distance, from the first to the 10th nn. In Fig. 2, the bonds and corresponding pair correlators are represented for the (1nn), $(1nn)^2$, and $(1nn)^3$ kinetic shell approximations. From the adiabatic approximation applied to the pair correlators $S_{i,n}^{AV}$ and $P_{i,n}^{AV}$ with $(n = 1,2,3,4a,4b,5,7a,7b,10)$ and the use of Eqs. (10) and (13), we deduce that the Fourier transforms of the pair correlators are a solution of the linear system of equations

$$q_0 T U_k = -B, \tag{B1}$$

where U_k is the Fourier transform of vector U_i. All coordinates of vector B are null but the first one,

$$B_1 = 2c_B L_{AA}^{(0)}\lambda(k)\delta\mu_{AV} - 2c_A L_{BB}^{(0)}\lambda(k)\delta\mu_{BV}. \tag{B2}$$

The matrix T is equal to $T = R + \mathrm{Diag}(D)$ with R given by

$$\begin{pmatrix}
0 & 0 & \lambda_k^1 & \lambda_k^2 & 4\lambda_k^4 & 2\lambda_k^1 & 2\lambda_k^2 & 2\lambda_k^4 & 0 & 0 & 0 & 0 & \lambda_k^1 & \lambda_k^2 & 0 & 0 & 0 & 0 & 0 & 0 \\
0 & 0 & \lambda_k^2 & \lambda_k^1 & 4\lambda_k^3 & 2\lambda_k^2 & 2\lambda_k^1 & 2\lambda_k^3 & 0 & 0 & 0 & 0 & \lambda_k^2 & \lambda_k^1 & 0 & 0 & 0 & 0 & 0 & 0 \\
4\lambda_k^3 & 4\lambda_k^4 & 0 & 0 & 0 & 0 & 0 & 0 & 0 & 0 & 4\lambda_k^1 & 4\lambda_k^2 & 0 & 0 & 0 & 0 & 0 & 0 & 0 & 0 \\
4\lambda_k^4 & 4\lambda_k^3 & 0 & 0 & 0 & 0 & 0 & 0 & 0 & 0 & 4\lambda_k^2 & 4\lambda_k^1 & 0 & 0 & 0 & 0 & 0 & 0 & 0 & 0 \\
4\lambda_k^2 & 4\lambda_k^1 & 0 & 0 & 0 & 0 & 0 & 0 & 4\lambda_k^2 & 4\lambda_k^1 & 0 & 0 & 0 & 0 & 0 & 0 & 0 & 0 & 0 & 0 \\
2\lambda_k^3 & 2\lambda_k^4 & 0 & 0 & 0 & 0 & 0 & 0 & 2\lambda_k^3 & 2\lambda_k^4 & 2\lambda_k^1 & 2\lambda_k^2 & 0 & 0 & 0 & 0 & 2\lambda_k^1 & 2\lambda_k^2 & 0 & 0 \\
2\lambda_k^4 & 2\lambda_k^3 & 0 & 0 & 0 & 0 & 0 & 0 & 2\lambda_k^4 & 2\lambda_k^3 & 2\lambda_k^2 & 2\lambda_k^1 & 0 & 0 & 0 & 0 & 2\lambda_k^2 & 2\lambda_k^1 & 0 & 0 \\
2\lambda_k^2 & 2\lambda_k^1 & 0 & 0 & 0 & 0 & 0 & 0 & 4\lambda_k^2 & 4\lambda_k^1 & 0 & 0 & 0 & 0 & 2\lambda_k^2 & 2\lambda_k^1 & 0 & 0 & 0 & 0 \\
0 & 0 & 0 & 0 & 2\lambda_k^4 & \lambda_k^1 & \lambda_k^2 & 2\lambda_k^4 & 0 & 0 & 0 & 0 & \lambda_k^1 & \lambda_k^2 & 0 & 0 & 0 & 0 & 0 & 0 \\
0 & 0 & 0 & 0 & 2\lambda_k^3 & \lambda_k^2 & \lambda_k^1 & 2\lambda_k^3 & 0 & 0 & 0 & 0 & \lambda_k^2 & \lambda_k^1 & 0 & 0 & 0 & 0 & 0 & 0 \\
0 & 0 & \lambda_k^3 & \lambda_k^4 & 0 & 2\lambda_k^3 & 2\lambda_k^4 & 0 & 0 & 0 & 0 & 0 & \lambda_k^3 & \lambda_k^4 & 0 & 0 & 0 & 0 & 0 & 0 \\
0 & 0 & \lambda_k^4 & \lambda_k^3 & 0 & 2\lambda_k^4 & 2\lambda_k^3 & 0 & 0 & 0 & 0 & 0 & \lambda_k^4 & \lambda_k^3 & 0 & 0 & 0 & 0 & 0 & 0 \\
\lambda_k^3 & \lambda_k^4 & 0 & 0 & 0 & 0 & 0 & 0 & 2\lambda_k^3 & 2\lambda_k^4 & \lambda_k^1 & \lambda_k^2 & 0 & 0 & \lambda_k^3 & \lambda_k^4 & 2\lambda_k^1 & 2\lambda_k^2 & \lambda_k^1 & \lambda_k^2 \\
\lambda_k^4 & \lambda_k^3 & 0 & 0 & 0 & 0 & 0 & 0 & 2\lambda_k^4 & 2\lambda_k^3 & \lambda_k^2 & \lambda_k^1 & 0 & 0 & \lambda_k^4 & \lambda_k^3 & 2\lambda_k^2 & 2\lambda_k^1 & \lambda_k^2 & \lambda_k^1 \\
0 & 0 & 0 & 0 & 0 & 0 & 0 & 2\lambda_k^4 & 0 & 0 & 0 & 0 & \lambda_k^1 & \lambda_k^2 & 0 & 0 & 0 & 0 & 0 & 0 \\
0 & 0 & 0 & 0 & 0 & 0 & 0 & 2\lambda_k^3 & 0 & 0 & 0 & 0 & \lambda_k^2 & \lambda_k^1 & 0 & 0 & 0 & 0 & 0 & 0 \\
0 & 0 & 0 & 0 & 0 & \lambda_k^3 & \lambda_k^4 & 0 & 0 & 0 & 0 & 0 & \lambda_k^3 & \lambda_k^4 & 0 & 0 & 0 & 0 & 0 & 0 \\
0 & 0 & 0 & 0 & 0 & \lambda_k^4 & \lambda_k^3 & 0 & 0 & 0 & 0 & 0 & \lambda_k^4 & \lambda_k^3 & 0 & 0 & 0 & 0 & 0 & 0 \\
0 & 0 & 0 & 0 & 0 & 0 & 0 & 0 & 0 & 0 & 0 & 0 & \lambda_k^3 & \lambda_k^4 & 0 & 0 & 0 & 0 & 0 & 0 \\
0 & 0 & 0 & 0 & 0 & 0 & 0 & 0 & 0 & 0 & 0 & 0 & \lambda_k^4 & \lambda_k^3 & 0 & 0 & 0 & 0 & 0 & 0
\end{pmatrix}, \tag{B3}$$

where the coefficients λ_k are

$$\lambda_k^1 = (1 + e^{-ikd})/2 \quad \lambda_k^2 = (1 - e^{-ikd})/2 \quad \lambda_k^3 = (1 + e^{ikd})/2 \quad \lambda_k^4 = (1 - e^{ikd})/2,$$

corresponding to the Fourier transforms of the spatial operators

$$\lambda_i^1(f) = (f_i + f_{i-1})/2 \quad \lambda_i^2(f) = (f_i - f_{i-1})/2 \quad \lambda_i^3(f) = (f_i + f_{i+1})/2 \quad \lambda_i^1(f) = (f_i - f_{i+1})/2, \tag{B4}$$

where f_i is the value of function f at site i.

The coordinates of vector D are

$$D_1 = -2\frac{q_2}{q_0} - (z-1) \quad D_2 = -(z-1) \quad D_i = -z, \quad \forall i \geqslant 3. \tag{B5}$$

[1] A. R. Allnatt and E. L. Allnatt, Phil. Mag. A **64**, 341 (1991).
[2] T. Garnier, M. Nastar, P. Bellon, and D. R. Trinkle, Phys. Rev. B **88**, 134201 (2013).
[3] T. Garnier, V. R. Manga, D. R. Trinkle, M. Nastar, and P. Bellon, Phys. Rev. B **88**, 134108 (2013).
[4] T. Garnier, D. R. Trinkle, M. Nastar, and P. Bellon, Phys. Rev. B **89**, 144202 (2014).
[5] A. L. Greer and F. Spaepen, in *Synthetic Modulated Structures*, edited by L. Leroy, B. Chang, and C. Giessen (Academic Press, Orlando, 1985), pp. 419–484.
[6] J. W. Cahn, Acta Metall. **9**, 795 (1961).
[7] J. W. Cahn, J. Chem. Phys. **42**, 93 (1965).
[8] J. W. Cahn and J. E. Hilliard, J. Chem. Phys. **28**, 258 (1958).
[9] J. W. Cahn, Acta Metall. **10**, 179 (1962).
[10] H. E. Cook, Acta Metall. **18**, 297 (1970).
[11] M. Hillert, Acta Met. **9**, 525 (1961).
[12] H. E. Cook, D. D. Fontaine, and J. E. Hilliard, Acta Metall. **17**, 765 (1969).
[13] R. Kikuchi and L.-Q. Chen, Nanostruct. Mater. **5**, 257 (1995).
[14] R. Kikuchi, L.-Q. Chen, and A. Beldjenna, Nanostruct. Mater. **5**, 269 (1995).
[15] A. G. Khachaturyan, *Theory of Structural Transformations* (Wiley, New York, 1983).
[16] H. E. Cook and J. E. Hilliard, J. Appl. Phys. **40**, 2191 (1969).
[17] T. Tsakalakos, Thin Solid Films **86**, 79 (1981).
[18] W. M. Paulson and J. E. Hilliard, J. Appl. Phys. **48**, 2117 (1977).
[19] T. Tsakalakos and J. E. Hilliard, J. Appl. Phys. **55**, 2885 (1984).
[20] G. Martin, Phys. Rev. B **41**, 2279 (1990).
[21] M. Plapp and J.-F. Gouyet, Phys. Rev. Lett. **78**, 4970 (1997).
[22] J. W. Cahn and J. E. Hilliard, J. Chem. Phys. **31**, 688 (1959).
[23] T. Tsakalakos and J. E. Hilliard, Metall. Trans. A **20**, 357 (1989).
[24] T. Tsakalakos, Scr. Metall. **15**, 255 (1981).
[25] R. Kikuchi, J. Phys. Chem. Solids **20**, 17 (1961).
[26] R. Kikuchi and H. Sato, J. Chem. Phys. **53**, 2702 (1970).
[27] M. Nastar, V. Y. Dobretsov, and G. Martin, Phil. Mag. A **80**, 155 (2000).
[28] M. Nastar, Phil. Mag. **85**, 3767 (2005).
[29] V. Barbe and M. Nastar, Phil. Mag. **86**, 1513 (2006).
[30] V. Barbe and M. Nastar, Phil. Mag. **86**, 3503 (2006).
[31] V. Barbe and M. Nastar, Phil. Mag. **87**, 1649 (2006).
[32] V. Barbe and M. Nastar, Phys. Rev. B **76**, 054205 (2007).
[33] V. Barbe and M. Nastar, Phys. Rev. B **76**, 054206 (2007).

[34] H. Sato and R. Kikuchi, Acta Metall. **24**, 797 (1976).
[35] H. Sato, K. Gschwend, and R. Kikuchi, J. Phys. Colloques **38**, C7-357 (1977).
[36] K. Gschwend, H. Sato, and R. Kikuchi, J. Chem. Phys. **69**, 5006 (1978).
[37] K. Gschwend, H. Sato, R. Kikuchi, H. Iwasaki, and H. Maniwa, J. Chem. Phys. **71**, 2844 (1979).
[38] J. K. McCoy, R. Kikuchi, K. Gschwend, and H. Sato, Phys. Rev. B **25**, 1734 (1982).
[39] M. Nastar, Phil. Mag. **85**, 641 (2005).
[40] Y. LeBouar and F. Soisson, Phys. Rev. B **65**, 094103 (2002).
[41] E. Clouet, M. Nastar, and C. Sigli, Phys. Rev. B **69**, 064109 (2004).
[42] E. Clouet, L. Laé, T. Épicier, W. Lefebvre, M. Nastar, and A. Deschamps, Nat. Mater. **5**, 482 (2006).
[43] G. Martin and C. Desgranges, Europhys. Lett. **44**, 150 (1998).
[44] A. Bortz, M. Kalos, and J. Lebowitz, J. Comput. Phys. **17**, 10 (1975).
[45] N. Metropolis, A. W. Rosenbluth, M. N. Rosenbluth, and A. H. Teller, J. Chem. Phys. **21**, 1087 (1953).
[46] C. Domb, in *Phase Transitions and Critical Phenomena*, edited by C. Domb and M. S. Green (Academic Press, London, 1974), Vol. 3, p. 425.
[47] M. Nastar and F. Soisson, Phys. Rev. B **86**, 220102 (2012).
[48] R. Wagner, R. Kampmann, and P. W. Voorhees, in *Phase Transformations in Materials*, edited by G. Kostorz (Wiley, Weinheim, 2001), Chap. 5.
[49] *Diffusion in Solid Metals and Alloys*, edited by H. Mehrer, New Series, Group 3, Vol. 26 (Springer Verlag, London, 1990).
[50] O. Senninger, E. Martinez, F. Soisson, M. Nastar, and Y. Bréchet, Acta Mat. **73**, 97 (2014).